Fault seal behaviour in Permian Rotliegend reservoir sequences: case studies from the Dutch Southern North Sea

K. van Ojik[1,*], A. Silvius[1,2], Y. Kremer[3] & Z. K. Shipton[3]

[1] EBN, Daalsesingel 1, 3511 SV Utrecht, The Netherlands

[2] State University Utrecht, Faculty Geosciences, Heidelberglaan 2, 3584 CS Utrecht, The Netherlands

[3] University of Strathclyde, Department of Civil and Environmental Engineering, 75 Montrose Street, Glasgow, G11XJ, United Kingdom

[*] Correspondence exploration@ebn.nl

ABSTRACT

Permian Rotliegend reservoir rocks are generally characterised by high N/G ratios, and faults in such sand-dominated lithologies are typically not considered likely to seal. Nevertheless many examples of membrane sealing are present in Rotliegend gas fields in the Southern Permian Basin. This manuscript reviews examples of membrane sealing in the Dutch Rotliegend, it presents an extensive dataset of petrophysical properties of Rotliegend fault rocks, and analyses two case studies using commonly used workflows.

Fault (membrane) seal studies have been carried out on two Rotliegend fields to test the level of confidence and uncertainty of prediction of Across Fault Pressure Differences (AFPD) based on existing SGR-based algorithms such as those by Bretan et al. (2003) and Sperrevik et al. (2002). From the field studies it is concluded that observable small AFPDs are present and that these are likely pre-production AFPDs due to exploration-time scale trapping and retention of hydrocarbons. Two SGR-based empirical algorithms have been used here to estimate AFPD's in lower N/G reservoir intervals with the aim to predict membrane seal behaviour and these results are compared to field data. It is concluded the selected SGR-based tools predict AFPD for Upper Rotliegend lower N/G reservoir rocks with reasonable results. Nonetheless the core sample data sets show a much wider range of permeability and capillary entry pressure than predicted by the selected SGR transforms. This highlights the potential to modify existing workflows for application to faults in high N/G lithologies. Data sharing and collaboration between industry and academics is encouraged, so that in the long run workflows can be developed specifically for faults in high N/G lithologies.

Introduction

Most gas producing fields in the Netherlands are situated in reservoirs formed by mixed aeolian and fluvial deposits of the Permian Upper Rotliegend Group. Since the discovery and development of the giant Groningen gas field (1959), the Rotliegend gas play is now considered a very mature play (EBN, 2017). Ongoing production of many fields towards and into the tail end of their production life has made apparent that discrepancies between the static and dynamic volumes are observed. These discrepancies are related to the presence of vertical baffles within those fields, presenting restrictions to pressure communication and therefore a certain level of compartmentalization, and are in most cases explained by the presence of (partly) sealing faults (van Hulten, 1996, 2010) or fault systems (Corona, 2005; Geiss et al., 2009). Examples of gas field compartmentalization and the presence of fault sealing have been described in various publications (Figure 1, Table 1). The publications outlined in table 1 clearly identify a high level of variation in fault styles and geometries, trends, and history. From above references it is concluded that, at a regional scale, fault sealing causes and mechanisms are understood, but that it remains difficult to predict fault seal on a smaller scale. Understanding the sealing behaviour of faults remains very important because many of the remaining economically attractive exploration prospects in the Dutch on- and offshore area depend upon structural closure defined by a spill point related to possible fault sealing. Additionally, it is equally important to understand the level of compartmentalization on a field production time scale to allow identification of the economically most attractive appraisal and development scheme, e.g. the number and position of wells to be drilled.

The term “fault seal” covers a range of situations in which flow across a fault is absent, or hampered, including those situations where (1) low permeability rock is juxtaposed against higher permeability rock at the fault face (juxtaposition sealing), (2) situations where faults support large hydrocarbon columns over geological time, and (3) those situations where faults act as minor or major production baffles. The most common usage of the term ‘membrane seal’ refers to those situations where fault sealing relies on capillary processes.

An overview will be presented here of Southern North Sea fields where the likely presence of membrane sealing has been confirmed by data collected in exploration and production wells (Figure 1), for example in the form of observed unexpected free water level depth differences across faults or the lack of dynamic pressure support across fault zones.

Then follows a summary and review of data from detailed core analyses carried out on a selection of fault and host rock samples carefully selected from well core material from Upper Rotliegend intervals, and which data has been used for calibrating existing predictive property transformation functions.

Thirdly, two case studies of Rotliegend fields from the Dutch offshore are presented where available data strongly suggests the presence of membrane sealing across major faults within the field. These case studies are (1) the L12B-C field (operated by Neptune Energy) and (2) an anonimised field in the Southern North Sea area, here referred to as field SNS-A. Data from these fields has been used to validate two commonly used fault rock property transformation functions, those of Bretan et al. (2002) and Sperrevik et al. (2002).

Geological setting of the Rotliegend Play

Stratigraphy and palaeogeography

The Rotliegend Gas Play (Figures 2 and 3) is a textbook example of the superposition of three key components of hydrocarbon plays: (1) prolific Late Carboniferous coal rich source rocks for gas; (2) laterally very extensive sheets of thick sandstones forming the Slochteren Sandstone reservoir; and (3) the thick and continuous evaporitic Zechstein presenting an almost perfect top seal (de Jager et al., 2007). The most prospective area for hydrocarbons is located in an east-west oriented fairway which stretches from the offshore United Kingdom across the Netherlands and Germany into Poland. Along the southern edge of the Southern Permian Basin this fairway is formed by the presence of a mixed fluvial and aeolian facies belt (Gast et al., 2010). Within the Netherlands, towards the North, the Rotliegend rapidly thickens. The centre of the Rotliegend Basin was formed by an East-West trending axis located across the northern part of the Dutch offshore, and where the largest total thickness of the Rotliegend has been attained in access of more than 1.5km. The northern boundary to the Southern Permian Basin is formed by an aligned series of highs, including the Mid-North Sea High and the Ringkøbing-Fyn High (Pharaoh et al., 2010).

Stratigraphically, the Upper Rotliegend (Figure 2) can be subdivided into at least two genetically linked depositional cycles, (1) a lower cycle bound by the top of the "transgressive" Ameland Member at the top, and the base of the Lower Slochteren at the base, the latter concurrent with the Base Permian Unconformity, and (2) an upper cycle bounded by the base of the transgressive Copper Shale at the top, and the top of the transgressive Ameland Member at the base, including the Upper Slochteren and Ten Boer Members, and their time equivalent deposits (van Adrichem Boogaert et al., 1993-1997; George et al., 1997; van Ojik, et al., 2011). The sand content within each of the claystone members shows a gradual increase towards the basin margin, and conversely the sandstone members demonstrate an increase in shale content in a basin-centre ward direction. The centre of the Southern Permian Basin is characterized by the deposition of thick series of claystones intercalated with halite beds deposited within the Silverpit lake, although this was more likely not one single lake, but a system of inter-linked smaller perennial saline ponds. Overall, the Rotliegend shows a pattern of increasing expansion of the Silverpit lake from old to young, and regressive patterns of gradual back-stepping depositional systems, causing the sand-prone deposits of the Lower Slochteren Member to be present further towards the North compared to the sand-prone deposits of the Upper Slochteren Member. Figure 3 shows the present-day distribution of the Upper Rotliegend deposits. Vshale, N/G, burial depth, and high porosity contours have been obtained by convergent interpolation and contouring of data from exploration and appraisal wells available.

Structural setting and burial history

An understanding of the fault and fracture systems present in the Upper Rotliegend rocks, their relation to fault rock and surrounding host rock properties and consequently sealing potential, requires an understanding of the regional tectonic evolution of the area of interest. We present a high-level overview here: for more detail the reader is referred to Ziegler (1990), Leveille et al. (1997), Corona (2005), Barr (2007), de Jager et al. (2007), Ligtenberg et al. (2011) and references therein.

An overview of typical seismically observable fault patterns in the Rotliegend is presented in Figure 4, which exemplifies the various phases of fault activity. A prominent fault trend is oriented in a NW-SE strike direction, and this trend is generally very pervasive, continuing for up to tens of kilometres. The NW-SE fault trend is generally linked with the deeper subsurface into reactivated basement-rooted fault systems, probably of Caledonian origin (Pharaoh, et al., 2010).

The Variscan Orogeny (ca 300 Ma BP) was associated with closure of the Proto-Tethys Ocean during the Carboniferous, with roughly north-south compression. NW-SE trending faults in the deeper subsurface are interpreted to represent this Variscan event. Post-orogenic tectonic activity in the latest Carboniferous and earliest Permian (ca 300 Ma BP) caused oblique-slip faulting and related thermal uplift causing large-scale exhumation of Carboniferous deposits, resulting in the creation of large-scale NE-SW and NW-SE conjugate fault systems (e.g. Geiss et al., 2008). These fault systems in Rotliegend deposits have gone through several phases of re-activation (Ligtenberg et al., 2011). Regional subsidence due to the ongoing relaxation of a weak and thin lithosphere resulted in the formation of the very large Southern Permian Basin (van den Belt, 2007), and provision of the accommodation space in which the sediments of the Upper Rotliegend system were deposited (van Ojik, et al., 2011). Continuing mild extension during the Permian occurred in a roughly East-West direction.

Transtensional stresses during the opening of the proto-Atlantic Ocean (Early-Cimmerian event, circa 230 Ma BP) were oriented in a roughly ENE-WSW direction causing a mild re-organization of the structural configuration of the Southern Permian Basin. Zechstein salt locally started to move in response to extensional events, showing an increasing decoupling of the mechanical response between the over- and under-burden of the Zechstein.

Ongoing break-up of the Pangaean supercontinent, associated with thermal uplift of the Mid North Sea High during the Early Jurassic is referred to as the Mid-Cimmerian event (ca 175 Ma BP). This is a generally NE-SW oriented transtensional phase and in which the main structural features of the Dutch subsurface formed are amplified in the development of large-scale graben systems such as the Broad Fourteens Basin, the Vlieland Graben, etc. Pulses of repetitive extension related to the ongoing opening of the Atlantic Ocean and break-up of Laurentia caused roughly east-west oriented extension of major graben systems, a phase referred to as the Late Cimmerian Event (ca 145 Ma BP). Decoupling of the structural response to tectonic activity between the Zechstein over-burden versus under-burden, and absence of Zechstein salt in the southern part of the Dutch on- and offshore, caused a strong contrast of structural styles in response to the Late Cimmerian event. In northern parts of the Southern North Sea, strongly continuous north-south trending faults in trend with the Dutch Central Graben can be observed at Rotliegend level, whereas in the South, where Zechstein salt is absent, the pre-existing structural grain was re-activated.

Closure of the Tethys Ocean, and collision of the African and Eurasian plates finally caused a series of compressional pulses during the Late Cretaceous and Early Tertiary. This lead to inversion of existing Upper Jurassic and Early Cretaceous Basins (De Jager et al., 2007). Seismic expressions of this compressional event are the local presence of reverse faults, (over) thrusting and pop-up features along major NW-SE trends. Conjugate NE-SW trending faults can be observed in which transfer movements accommodate some of the oblique inversion along the NW-SE trends. These NE-SW / NNE-SSW fault trends, referred to as 'Dekeyser' faults (Dekeyser, 1990), are linear and semi-continuous over large distances (50-100km's long) with only limited lateral offset. They show however apparent small throws close to or below seismic resolution. In places it is a major difficulty to accurately map and/or image these faults (Geiss et al., 2009). Several field studies have demonstrated these Dekeyser faults act as sealing faults over production time with Across Fault Pressure Difference (AFPD) in excess of 200 bar.

As described by Dekeyser (1990), these features appear to be parallel and regularly spaced (2-3km), with occasionally rather continuous collapse zones. Geiss et al. (2008, 2009) describe two geometries of these lineaments as seen on seismic: (1) as single, sub-vertical, fault planes sometimes with large throw, and (2) as two opposing fault planes creating narrow graben systems, also referred to as thin-skinned grabens (Vendeville et al., 1992) or skinny grabens (Leveille, et al., 1997), depending on their width (down to 1 seismic trace, i.e. less than 25m). Analysis of throw profiles shows strong variation on a hectometre scale, suggesting a more complex segmented structure at scales beyond the seismic resolution. Similar complex fault geometry observations are documented by Corona (2005) and Leveille et al. (1997) who also claim that evaporites may have infiltrated from the overlying Zechstein and therewith contribute to the sealing potential of these fault systems.

More detailed structural analysis of the Cleaver Bank High area (which in the North partly overlaps the area covered in Chen (2015), Schroot et al. (2003) and Oudmayer et al. (1993) support that NNE-SSW and NE-SW fault trends show anomalously high length-to-throw ratios and authors explain this by repetitive reactivation of much older Variscan fault structures during the Meso- and Cenozoic.

Field examples of membrane seals at Rotliegend level

Compartmentalization of Rotliegend gas accumulations was identified soon after the first Rotliegend gas fields came into production (van Hulten, 1996). Figures 1 and 3 and Table 1 document examples of membrane seals at Rotliegend level. Evidence for the presence of these membrane seals is provided by the presence of Free Water Level (FWL) depth and formation pressure differences across faults (at pristine conditions). For some of these fields there is no public data available to further follow up and better understand the importance of membrane sealing. Some more multi-disciplinary integrated and robust field (and fault) reviews were carried out where fields where studied in the light off all data available, including petrophysical analysis of fault rock data (see Table 1) subsequently used in material balance and dynamic production history matching calculations. A few proprietary field reviews are available to authors where empirical Shale Gouge Ratio (SGR)-based functions were used to predict fault capillary entry pressures and expected hydrocarbon column heights (see table 1). The SGR function is based on the average host rock clay content which passes the calculation point on the fault. The SGR estimate of the fault rock clay content is then used as a basis for fault rock property assessment. In the following it will be questioned if using the SGR algorithm is a valid assumption for faults in high N/G Permian Rotliegend reservoir rocks, in particular in view of the fault displacement processes.

Fault seal prediction

In the hydrocarbon industry, fault seal studies play an important role in the evaluation of hydrocarbon traps to understand cross fault flow and retention capacity, not just over geological time scales (most relevant for exploration), but also over production time scales in relation to field compartmentalization and differential depletion. Several fault seal analysis techniques have been developed in last decades with subsequent minor modifications since. The most common methodology consists of (1) the construction of a discrete fault and horizon framework model, based on seismic interpretation, and their related horizon-fault and fault-fault intersection lines, (2) careful geometrical analysis to make a distinction between areas of juxtaposition sealing (where reservoir rock is juxtaposed against non-reservoir rock at the fault face), and potential leak windows at areas of reservoir-reservoir juxtaposition (Allan, 1989; Knipe, 1997) and (3) a prediction of the height of the hydrocarbon column that can be maintained by the fault seal through the process of membrane sealing (Bretan, 2017). Ideally, fault properties such as permeabilities and entry pressures based on core data are used for these prediction, but such data are typically not available due to the lack of core material. In areas and intervals with a higher variability in N/G ratios the maximum hydrocarbon column height is typically estimated based on the fault displacement and clay content of the host rock using the SGR algorithm (Bretan et al., 2003), or comparable type of transformation (Lindsay, et al., 1993; Yielding et al., 1997; Yielding, 2002; Freeman, et al., 2010).

The SGR algorithm is a very useful approach for conditions with lower N/G rocks where shale rich rocks will be incorporated into the fault zone. In case of higher N/G rocks different displacement processes will take place including grain reorientation, crushing, dissolution and cementation of quartz or other diagenesis and which will affect fault properties, which is beyond the application of SGR. Stress and temperature in relation to geo-history play a very significant role here but relevant data of the evolution of fault rock properties with temperature and pressure is currently limited available to study and understand this better.

Upper Rotliegend reservoir sediments of the Southern Permian Basin are typically high N/G rocks, and fault characterization based on visual inspection of core material in the form of slabs and chips suggests that these faults are indeed dominated by the presence of deformation bands and cataclasites formed under complex structural conditions (Mauthe, 2003; Fisher et al., 2005; Ligtenberg et al., 2011; Busch, et al., 2015). It should be noted that these observations are generally made on relatively small scale structures (centimetres of displacement), which are not necessarily representative for the properties of seismic scale faults. Seismic scale faults interact with a greater amount of stratigraphy, so they are more likely to intersect sparse shale beds than cm scale fractures. Kremer et al. (in press) show from outcrop data that shale beds are not well mixed in large fault zones and can therefore play a disproportionate small role in clay smearing and fault seal behaviour. The dominance of cataclasis in the dataset, the examples of observed AFPDs for faults with reservoir-reservoir juxtaposition of high N/G rock, and the poorly constrained property prediction at low SGR values poses the question if current shale gouge or clay smear functions should be used to predict sealing capacity of fault and fracture systems hosted in the Upper Rotliegend. The goal of this paper is to share some observations with respect to the limitiations of output of certain publicly available transformations and the need to better understand the evolution of faults and fractures in relation to their surrounding host rock properties and pressure and temperature history.

Fault rocks

The petrophysical properties of fault rocks (e.g. permeability, capillary entry pressure) are fundamental factors controlling the ability of fault rock to sustain pressure communication across the fault. These petrophysical properties depend upon a large range of subsurface processes including variations in sediment composition, stress and temperature history during the complex geological history of the Southern North Sea Basin (Fisher et al., 1998).

Cataclasis and deformation bands

Subsurface data across various scales (including seismic data, borehole image logs and well cores) have revealed that faults in the area of interest are frequently composed of or associated with a zone of larger and smaller faults and fractures referred to as fault damage zones (e.g Frikken, 1996; Fisher et al., 1998; Ligtenberg, et al., 2011; Busch et al., 2015) with inherent vertical and horizontal permeability variations. One of the intrinsic problems with these subsurface data is the limitation of integration of observations and data into robust concepts across the various scales. Up- and downscaling of fault rock properties (notably permeability) would ideally allow to confident prediction of transmissibility multiplier ranges used in dynamic modelling for production history matching and forecasting. This would require however a representative set of wells drilling through a seismically resolvable fault zone whilst acquiring necessary data across that fault zone such as core, image logs, wireline data which data is very limited available in the public domain.

For the current purpose of understanding permeability and fluid flow through a fault zone, representing a series of deformation bands in porous rock, the subdivision provided by Fossen et al. (2007) is considered most useful. Their classification is based on the dominant deformation mechanism, allowing the identification of four principal types and which terminology will be used in current paper. These four types are:
(1) disaggregation bands, which form in a granular flow process in which grain rolling, boundary sliding and minorbreaking occurs
(2) phyllosilicate bands, where clay minerals promote grain boundary sliding
(3) cataclastic bands, which occur when grains fracture and break (Aydin, 1978) and
(4) solution and cementation bands, where dissolution and cementation occur along a deformation band..
Different deformation mechanisms produce bands with different petrophysical properties, such as permeability and threshold pressure, which are relevant parameters into modelling membrane seal behaviour.

On a core scale, the various fracture types observed include deformation bands (including cataclastics), cemented fractures, shale smears, phyllosilicate framework faults, and open fractures, albeit the most common types in the Upper Rotliegend are cataclastic and cemented fractures (Ligtenberg et al., 2011). Detailed core laboratory analysis of fractures in cores (see further in this paper) has shown that both cemented and cataclastic fractures have the potential to hold significant pressure differences.

Deformation bands experience strain hardening, and therefore they can only accumulate very limited offsets (centimetres at most). Progressive deformation is first accommodated by the formation of multiple deformation bands (e.g. Antonellini et al., 1994; Shipton et al., 2001, 2003) after which localization of deformation leads to clustered zones of deformation bands. Subsequent deformation of these zones leads to the development of slip surfaces and the formation of cataclastic fault cores of centimetre to metre scale thickness. This architecture consisting of a fault core consisting of cataclasites, clustered deformation bands and slip surfaces, surrounded by a damage zone with deformation bands is representative for many seismic scale faults (>20m offset) in porous sandstone. Both the damage zone and the fault core can therefore act as a barrier or baffle to across fault flow, while at the same time, a well-developed slip surface can act as a pathway for along-fault fluid flow (Shipton et al., 2002).

Diagenesis and cementation

Cataclastic bands are the dominant fault rock reported within core from the Rotliegend (Leveille, et al., 1997; Mauthe, 2003; Fisher et al., 2005; Barr, 2007) . Grain-fracturing induced porosity collapse and alongside enhanced quartz cementation has resulted in these cataclastic faults having lower permeabilities and increased threshold pressures compared to the surrounding host reservoir rock. It should be noted that other diagenetic minerals such as anhydrite, barite and carbonates are encountered within Rotliegend faults. Grain-size reduction caused by shearing facilitated pervasive quartz cementation, promoted by the large grain surface area and availability of reactive fractured surfaces, see Knipe et al. (1997), Fisher et al. (1998, 2000) and Lander et al. (2014) for more details. Quartz solution and re-precipitation may start at temperatures around 70°C and typically accelerates where deformation takes place at temperatures greater than 90°C (Walderhaug, 1996; Leveille et al., 1997).

Microscopic-scale measurements of fracture properties

Core analysis data and images are available from fault samples (Table 2) from wells across the UK and Dutch offshore and Dutch and German onshore, including measurements of fracture and host rock permeability and mercury injection capillary pressures (Table 3). Some of those data have been published earlier (Leveille et al., 1997, Mauthe, 2003). Use of data measured by Fisher et al. (2005, 2006) in this paper has been approved by operators NAM and Total (and partners) (Appendix 1) and includes measurements of porosity, permeability, Mercury injection pressure on both host rock and fault rock core samples, clay content estimates based on XRD analysis and various thin section and SEM imagery. Data used by Barr (2007) was unfortunately not publicly available, and values have been estimated from figures in that paper.

Permeability

Based on the available petrophysical data from selected samples (Figure 5) the fault rock permeability at core plug scale varies from 0.001 to 0.05 mD (geometric mean minus/plus one standard deviation) and this range of permeability will depend upon the level of intensity of cataclasis and cementation. Permeabilities measured in fault rock specimens here are a 2-4 orders of magnitude of lower than the host rock (Figure 6).

Empirical transformations for fault seal prediction used within the context of this study (Bretan et al., 2003, Sperrevik et al., 2002) are typically based on host rock clay content and fault rock permeability or injection threshold pressure relations, albeit these empirical relationships are based on core rock and field data from the Brent province. These Brent rocks are much younger (Middle Jurassic) and have been deposited in a shallow marine, marginal marine and non-marine environment hence have a different petrographical composition and are typically lower N/G rocks with higher amounts of clay minerals. In addition they have been subject to a different burial history than the Rotliegend. Output of SGR based algorithms such as those by Bretan et al. (2003) and Sperrevik et al. (2002) under more poorly constrained conditions of low SGR values should therefore be used with care to predict membrane seal capacity in Rotliegend rocks.

A cross-plot of fault rock permeability against clay content for Rotliegend fault rocks is provided in figure 7, several SGR-based transformations are included as lines. The spread in permeability of cataclastic samples is likely associated with the level of cataclasis and deformation in those samples, but requires further study to allow firm statements. The limited number of samples within cemented samples appear to group together.

Transformations based on SGR such as provided by Jolley et al. (2007), Manzocchi et al. (1999), Sperrevik et al. (2002) and Bretan et al. (2003) typically aim to predict fault permeability, which then subsequently is transferred in transmissibility multipliers for dynamic simulation. This transfer is based on parameters such as fault throw and fault width with inherent uncertainty difficult to quantify given the current limited resolution of seismic data. In addition, re-organisation and/or amplification of fault and fracture networks due to other tectonic events such as the Late Cretaceous inversion event are not taken into account here. Validation of these fault seal models can then be carried out through dynamic history matching and (flowing) material balance calculations.

Mercury injection threshold pressure

The mercury injection results from the cataclastic faults collected over the last decades and available for the current evaluation show a considerable range between 4.24 – 40.8 bar (geometric mean minus/plus one standard deviation, but reflects samples with varying intensity of cataclasis and deformation. Injection threshold pressures corrected for in-situ conditions (Adams, 2016) are plotted against modelled maximum burial depth (Nelskamp et al., 2014) at which rocks have been buried during their geological history (Figure 8). Inclusion of AFPD data from lower N/G rocks from the two case studies presented within this paper (L12b-C and SNS-A) plot out of trend and are difficult to reconcile with the available petrophysical core rock measurements, which are dominated by cataclastic faults from higher N/G conditions.

Available injection threshold pressure data from core rock material (Fisher et al., 2005, 2006) plotted against average host rock clay content of those samples with SGR-based empirical relationships provided by Bretan et al. (2003) and Sperrevik (2002) in backdrop (Figure 9) yields no correlation at all. This once again supports that output from SGR-based algorithms are probably invalid for fault seal predictions in high N/G Rotliegend reservoir rock which are likely dominated by cataclastic faults.

Methodology

Validity of output of transformations and functions

At Rotliegend field scale, membrane seal calculations are frequently made for those situations where there is gas fill on both sides of a fault, but where the FWL is different on both sides of a fault. Underschultz (2007) described three fundamentally different pressure patterns for this situation. In this paper we will focus on his Case 9 (discontinuous gas phase and different FWL's on both sides of a fault, but a constant water pressure gradient), as there are no Rotliegend fields in the Netherlands with tilted FWLs, and only one or two fields with active aquifer support. This situation (Case 9) is caused when the aquifer is hydraulically connected around or through the faults below the FWL (Figure 9).

For the assignment of properties to dynamic grid cell boundaries that represent fault planes, and subsequent translation into grid cell transmissibility multipliers, two different types of properties may be numerically estimated: fault permeability and threshold pressure. As previously explained the modelled capillary entry pressure of the fault plane (and consequently the maximum gas column height) equates to the amount of AFPD (at virgin conditions) which can be relatively easy validated in the presence of reliable pressure data collected in wells drilled on either side of a fault (Figure 10). For the current project it has been decided to focus on and validate the algorithms established by Bretan et al. (2003) and Sperrevik et al. (2002) since these two algorithms are available in the most commonly used fault seal evaluation software, and to our experience they're the most frequently used algorithms.

Predicting the maximum gas column height at either side of the fault is usually based on the transformation of the shale content of the fault-zone, expressed as SGR to injection threshold pressure. At least three different relationships have been published in literature (Bretan, 2017; Yielding et al. 2010) and are based on: (1) the empirical relationship between clay content of the host rock, amount of fault throw, burial depth and the AFPD (at same reference depth level on either side of the fault) (Bretan et al., 2003); (2) the empirical relationship between clay content and the threshold pressure derived from laboratory based injection tests on fault-rock samples extracted from core (Sperrevik et al., 2002); and (3) the empirical relationship between clay content, fault throw and buoyancy pressure ((Yielding et al., 2010).
Two case studies of Rotliegend fields are included in this paper for which the empirical relationships between

shale content, fault throw and AFPD based on Bretan (2003) and Sperrevik (2002) functions have been calibrated and validated against actual well and field data. Based on those two functions, and the average distribution of Rotliegend reservoir properties required for those functions ($5\%<Vf$, $SGR<25\%$, $2500m<Zf$, $Zmax<4500m$) it is expected that the capillary entry pressures and therefore AFPD ranges may vary between 2-16 bar (Sperrevik) and 0-4 bar (Bretan) (where SGR is Shale Gouge Ratio, Vf is the shale volume, Zf burial depth at which fault structural deformation occurred and Zmax the maximum burial depth).

Case studies

Data from the two Rotliegend gas fields presented here have been studied in more detail and compared to outcomes of two SGR-based empirical relationships between clay content of the host rock, and the AFPD, notably those by Bretan et al. (2003) and Sperrevik et al. (2002). These two fields are L12b-C (operated by Neptune Energy) and SNS-A (anonymized) which are both located in the Dutch offshore area (Figure 4). These fields have been selected based on the availability of sufficient data, including wells positioned on either side of a (partially) sealing fault, relevant well data including wireline logs (Gamma-ray, sonic and density logs), formation test pressure data, and historical production data. Both fields are covered by 3D seismic of good imaging quality. The L12b-C top reservoir is buried to a present-day depth of circa 3km, the top reservoir of SNS-A to circa 4.5km, allowing the comparison of results of, in particular, Sperrevik's function, which strongly depends upon maximum burial depth and reconstructed depth at time of deformation.

Case study 1 (L12b-C)

The L12b-C field, operated by Neptune Energy, is located circa 5km from the coastline. The trap is a combined fault-dip closure, with several fault blocks of Upper Rotliegend sandstone reservoir below a thick sequence of Zechstein evaporites. The field was discovered in 1979 with exploration well L12-3 drilled by NAM into the northern fault block of the field. Appraisal well L15-4 was drilled in the Middle/Southern domain within the same structural closure, and pressure data acquired suggest the presence of a different, deeper FWL from the northern block. In L12b-C the reservoir sequence is formed by the presence of an 'upper' (Slochteren B) and 'lower' (Slochteren D) sand-prone unit sandwiched between more clayey units (Slochteren A, C and E) in the Upper Slochteren Mb. (Figure 11) within the gas column. A considerable amount of thorough research has been carried out by current and previous operators to understand the dynamic behaviour of the field, which is partly captured by Weijermans et al. (2016).
The field was taken into production after drilling the L15-FA-106 well (abbreviated to A106 well here) in the northern compartment close to the subsurface location of the original L12-3 discovery well in 2000. The northern compartment is now (2018) depleted to a reservoir pressure of circa 50 bars. In 2014 a second producer (L15-A-108A, abbreviated to A108A here) was drilled into the central part of the field encountering significant pressure depletion of up to 50 bars (Figure 12) which can only be attributed to pressure depletion in the northern compartment.

The current case study comprises a high-level cross-check of available data against SGR-based algorithms to verify an alternative scenario in which a membrane seal is introduced between Northern and Middle segment. Available wireline gamma-ray data has been translated into a Vshale curve and combined with lithology interpretations from cuttings descriptions this enables a discrete subdivision of rock into 3 classes: “sand” (Vsh ≤ 0.4), “silt” (0.4 < Vsh < 0.5) and “shale” (Vsh ≥ 0.5). Reservoir sections are predominantly composed of rocks with low Vsh values, but a significant amount of shale is present within the complete section. It is possible these shales may be taken up in fault zones hence an SGR-based approach might work here.
The juxtaposition triangle plot of the critical fault between northern and middle segments (Figure 13) is based on the lithological subdivision of well L12-3 and suggests that at fault throws between 0 – 10m the sandy Slochteren B, and between 0-20m Slochteren D units, are self-juxtaposed. At fault throws between circa 20-50m the Slochteren D in the hanging wall block is juxtaposed against Slochteren B in the foot wall block. At fault throws between circa 10-30m and between 50-60m there are mainly juxtapositions of good sandy reservoir rock against silty rock with worse reservoir quality and hence limited likely across-flow capacity at the fault face. At fault throws larger than circa 60m there is no relevant reservoir rock self-juxtaposed across the fault and therefore the fault will act as a juxtaposition seal for cross fault seal. Vertical seismic resolution is around 20-30 meters hence introduces a significant uncertainty to amount of throw.
Cells of a 3d grid (width:length:height of cells ~ 50x50x1m) were populated with a discrete lithology based on the extrapolation of upscaled Vshale properties at the intersection of wells with the 3D grid, by using a lithology subdivision as above. This lithology grid was used to identify a juxtaposition property at each of the fault faces available in the 3D grid resulting in 6 different lithology juxtaposition combinations. Figure 14 shows a view towards the North at the fault face of the East-West oriented fault dividing the Northern and the Central domain, with nearby wells A108A (in front of the fault) and L12-3 and A106 behind the fault. Analysis of th 3D seismic indicates that across a significant part of the fault the Slochteren B and D are self-juxtaposed above the FWL, but also that roughly between the A108 and L12-3 well an area with significant fault throw exists in which the Slochteren B (“upper Sand”) in the hanging wall block in the South is juxtaposed against the Slochteren D (“lower Sand”).

Several formation pressure data points have been acquired in the various wells within the L12b-C field, both at virgin conditions, and at a time of significant pressure depletion in the Northern Domain, allowing the interpretation (within reasonable uncertainty limits) of the gas pressures and gradients within the field (Figure 15). Due to the absence of reliable pressure data from the aquifer, the hydrostatic pressure gradient has been interpreted based on data from nearby fields (L12b-A, L12b-B). This in turn has allowed for the interpretation of FWLs, and consequently based on wireline log evaluation and special core analysis data, the gas saturation profiles and depth of the Gas Water Contacts (GWC’s) (See (Weijermans et al., 2016) for a more detailed interpretation). Based on the presence of different FWLs on both sides of the dividing fault between the Northern and Middle Domain an AFPD of circa 4 bar can be reconstructed.
Based on the conversion of Hg-injection threshold pressure data of Rotliegend fault rock material explained

earlier (after Fisher et al., 2005), an AFPD of less than 3 bar (at in-situ conditions for gas-water system) would be expected under the current conditions (at relatively shallower present-day burial depth of circa 3km). The observed AFPD of 4 bar slightly exceeds that depth trend. It is worth noting that measured permeability data from fault core material from deformation band dominated faults in Utah is lower than deformation bands from the same fault's damage zone (Shipton et al., 2002), due to more intense cataclasis in the core alongside local grain contact quarts dissolution of quartz. It may be reasonable to assume that similar intensification of permeability reducing (and capillary pressure increasing) processes is taking place within the fault core of the Rotliegend faults.

Previous interpretations of the FWLs and the level of expected pressure equilibrium across the field prior to drilling the L15b-A108A well were explained by the operator through a model in which the fault between the Northern and Central Domain was fully closed (Weijermans et al., 2016). In this model, after initially sharing the same (paleo-) FWL across the field, the Northern and Central/Southern domains became isolated due to strike slip movement probably of Late Jurassic age (ca 150 Ma BP) and resulting cataclasis at the dividing East-West trending fault(s). Structural tilting and/or seal breaching in the northern compartment then caused different FWL's and possibly the presence of gas composition variations across the field. In addition, depth differences in the GWC and consequently transition zone between FWL and GWC have been explained by Weijermans et al. (2016) to reflect strong permeability variations across the field, deteriorating from North to South. Formation pressure data collected in well B108B however proved not only the presence of different FWLs, but also a significant amount of pressure depletion due to production in the Northern Domain. These data strongly resemble a situation described earlier by Underschultz (2007) in his Case 9, a model in which discontinuous gas phases and different FWL's on both sides of a fault are present, but at a constant hydrostatic pressure gradient. Gas phases are in the L12b-C field in pressure equilibrium due to the presence of a membrane seal acting as a valve with capillary entry pressure of circa 4 bar.

Seismic imaging quality of the fault between the Central and Southern compartment is rather limited, and an alternative concept can be presented in which the reservoir section of the L15-4 appraisal well has been drilled North of that fault, in the Central Domain. In this alternative concept, the fault between the Central and Southern Domain is trending in an almost East-West direction, structurally very similar to the sealing fault between the Northern and Central Domain, suggesting these two faults may have gone through a similar geological history, hence exhibiting comparable fault rock properties and thus sealing potential. Provided reservoir rock self-juxtaposition is present across that fault within the gas column, it is plausible to suggest that any gas within the Southern Domain is in pressure communication with the Central Domain, albeit across a membrane seal potentially causing different gas phases and FWLs on both sides of that fault, similar to the situation encountered in the Northern part of the field.

Empirical functions to estimate the seal failure envelopes relating SGR to fault zone capillary entry-pressure as a function of burial depth (Bretan et al.,2003) and depth of deformation (Sperrevik et al., 2002) have been compared against the observed field data (Figure 16).

It appears that both functions plausibly predict capillary entry pressure levels within the expected uncertainty ranges, although under base case conditions the function by Bretan (2003) slightly under-estimates the threshold pressure (minimum capillary entry pressure of 2 bar versus AFPD of circa 4 bar) and the function by Sperrevik (2003) slightly over-estimates it (minimum capillary entry pressure of circa 5 bar versus AFPD of circa 4 bar). It should be noted that here only the uncertainty ranges due to variations in clay content have been included. The function by Sperrevik relates seal failure to laboratory based Hg-injection entry pressure measurements and thus includes a conversion to gas-water subsurface conditions including the interfacial tensions of air-mercury and gas-water. The gas-water interfacial tension however is not accurately measured here and may range between 40-60 dyne/cm thus introducing an additional uncertainty.

From this case study it is concluded that within the L12b field a membrane seal could be present between the northern and middle segment. SGR based algorithms of Bretan (2002) and Sperrevik (2003), which could work here in view of lower variation in fault rock permeability at higher clay conetnts within the section , predict AFPD reliably compared to measured AFPD.

Case study 2 (SNS-A)

Despite anonymisation of this case study due to data confidentiality it has been added here as it offers possibly a view on membrane seal capacity at larger burial depth (between circa 4500 and 4600m) and associated with larger formation pressure and temperature compared to the previous case study. The 'SNS-A' field is located circa 60km northwest from the Dutch coastline. The trap is formed by a combined 3-way dip and fault closed structure and comprises several compartments. The relevant compartments here are referred to as SNS-A-BX and SNS-A-BY. The reservoir sequence of SNS-A is provided by mixed fluvial and aeolian sandy deposits of the Lower Slochteren Mb, overlain by sealing claystones of the Silverpit Fm, and evaporitic sequences of the Zechstein Gp. The SNS-A gas field was initially appraised with well WA, drilled into block BX.

Appraisal well WB was drilled a year later in the southern part of the BY block, 4 years later followed by production well WC. WC well was temporarily suspended due to technical problems and re-entered one year later to be completed as production well WD into the northern part of the BY block (see schematic base map of the field in figure 17). Both blocks have been taken into production, albeit block Y 6 years later after block BX. The producing sequence is formed primarily by a circa 60m sequence of mixed fluvial and aeolian sandstone (Figure 18), informally classified as Slochteren Alpha, within circa 125m thick, fining upwards sequence of sand- and siltstones classified as Lower Slochteren Member (van Adrichem Boogaert et al., 1997). Sandstone beds encountered within the underlying Carboniferous Limburg Group are occasionally situated within the gas leg and contribute to the in-place volumes. Possible contribution to flow and production has not been investigated by authors. The Slochteren Alpha is a high N/G sandstone but significant shale intercalations are present based on inspection of core images and wireline data. It is expected that deformation bands are primarily present in the form of cataclasites and with subordinate amounts of phyllosilicate rich deformation bands around those shale intervals. The presence of shale could lead to clay smearing into the fault zone, which has not been investigated in detail here.

The field is fully covered by 3D seismic data with sufficient sub-salt imaging quality to identify principal faults and horizons. The structural framework is characterized by the presence of a conjugate set of NW-SE and NE-SW trending faults. The BX and BY compartments are primarily fault closed structures with dip closure towards the North. A NE-SW trending fault forms the boundary between the BX and BY segments and has been focus of attention in the current study.

The fault offset is largest at the center of the fault (maximum 200m) and tapers to small offsets towards both the NE and SW tips (minimum observable offsets within the 3D seismic are around 30 metres). With an average reservoir thickness of circa 30m, self-juxtaposition of the Slochteren Alpha reservoir unit across the fault can be observed at both tips of the fault, although only the self-juxtaposed area in the SW is elevated above the FWLs. The impact of seismic resolution has not been investigated here. Based on the assumption of the presence of a hydrostatic pressure gradient similar to pressure gradients measured in the nearby exploration wells and the presence of pre-production pressure data in well WA has allowed to interpret a FWL in BX segment at circa 4730m True Vertical depth below sea level (tvdss) (Figure 19). Formation pressure data representative for the BY compartment has been collected in the WB well albeit 1 year after starting production in the adjoining BX segment, allowing the observation of a pressure difference between the wells of circa 4 bar (±1 bar). Several interpretations to explain the observed AFPD are presented here. First of all the AFPD could be caused due to pressure communication either across the fault or through the aquifer around the fault and therefore pressure depletion (ca 4 bar) in the BY segment, at which point in time the level of pressure depletion in BX segment was slightly more than 36 bar. It is expected that pressure transfer between the two compartmentments should be visible in the pressure and flow data for both segments, which is however likely not the case during the first years of production. In addition, very little vertical variation in depletion at start of production are observed which would be expected in the presence of vertical reservoir heterogeneity, such as demonstrated to be present based on the pressure data collected later in well WC.

An alternative interpretation explains the AFPD at the bounding fault due to membrane sealing between compartments in virgin, pre-production conditions. Well WC was drilled in the BY segment 6 years after start of production in the neighboring BX block (then depleted with circa 270 bar) clearly demonstrating (differential) pressure depletion of circa 45-55 bar across several reservoir layers supporting the hypothesis of the presence of a semi-permeable fault with (limited) pressure communication across that fault. Capillary entry pressure levels of this fault have been calculated based on functions by Bretan et al. (2003) and Sperrevik et al (2002), and compared against actual AFPD measured in wells (Figure 20). It is likely SGR-based predictions may be valid only for limited fault face areas where intercalated shale layers have been ripped up and shale particles incorporated into the deformation bands.

Based on these assumptions, the capillary entry pressure profile estimated with function by Bretan et al. (2003) is in good agreement with the measured AFPD. The pressure profile predicted by Sperrevik function significantly overestimates the membrane seal potential of the fault. A sensitivity analysis carried out indicates the strong dependence of this latter function on primary variations and uncertainty in the maximum burial depth. In addition, few data with a present day burial depth deeper than 4km where available to Sperrevik et al. (2002) for their analyses hence their functions are less calibrated and output may not be suitable for the depth domain of current SNS-A field.

Discussion and Conclusions

Tasks of a fault seal analysis workflow

As explained earlier, common tasks within a methodology to identify the presence of membrane seal (Knipe et al., 1998; Bretan, 2017) consist of at least (1) the construction of a discrete fault and horizon framework and the identification of several populations and generations of faults and their mutual relationships, (2) careful geometrical analysis to make a distinction between areas of juxtaposition sealing and areas of membrane sealing and (3) a prediction of the pressure difference (and associated hydrocarbon column height) that can be maintained through the process of membrane sealing. Within the current case studies we have focused particularly on the last task with the aim to predict AFPDs using two SGR-based algorithms. This has been done under conditions where there is actual well data control in the fields selected to compare the predicted AFPD to reservoir pressure data collected in those wells.

The first task of constructing a fault and horizon framework normally incorporates a detailed structural interpretation of the 3D seismic data available with the aim to understand relationships between the various fault generations through geological time and space. Within the Rotliegend this is a far from trivial task due to the inherited complex tectonic history, the repetitive re-activation of faults and fault systems in the presence of strong vertical geomechanical heterogeneity and discontinuity and the limitation of insufficient data availability or lack of resolution to resolve in detail structural deformation mechanisms (i.e. fault movement directions and amount of throw, timing, internal fault fabric, etc). Several field studies have demonstrated certain fault generations (Dekeyser lineaments) may act as sealing faults over geological time with AFPDs in excess of 200 bar, and which cannot yet be satisfactorily explained. The amount of net displacement across these Dekeyser lineaments will be relatively small, but with very significant amounts of displacement within the small (skinny) graben on the two opposing fault faces of these lineaments, cancelling out on a slightly larger scale. On a seismic scale, these lineaments are at or below resolution and hence generally mapped as one single event with small offset. Fault throw within the graben system is therefore not captured within the fault interpretation, consequently leading to a possible misjudgement of the amount of juxtaposition sealing, or an under-estimate of fault throw, and consequently any sealing properties that are modelled as an SGR-based function of throw. SGR based functions are therefore not applicable for predicting the level of fault (membrane) sealing associated with these Dekeyser lineaments if offset and cross-fault juxtaposition is unknown.

The second task involves a careful geometrical analysis to identify areas of juxtaposition versus membrane sealing for example with Allan diagrams including impact of (sub)seismic vertical and horizontal resolution. This process helps to clarify and quantify the vertical and horizontal distribution of juxtaposition seal as a function of reservoir depth and thickness versus fault throw, which is not necessarily a linear relationship.

A third task embraces a prediction of the expected level of membrane sealing and associated pressure difference which is maintained across the fault during geological time. SGR based functions evaluated here are established and calibrated against more clay prone shallow marine sediments of Middle Jurassic age from the Brent area (Central North Sea). They attempt to evaluate the cumulative effect of processes incorporating shale into the fault core (i.e. the bulk effect of processes such as shale abrasion, formation of disaggregation and phyllosilicate deformation bands). It is expected these processes will only play a role in Rotliegend rocks in the proximity of substantially thick shale layers and mixing of clay into the fault zone, hence SGR-based algorithms should be used under these conditions only.

Cataclastic deformation bands are most likely the dominant fault rock present within high N/G Rotliegend (sandstone) rock sequences. In outcrop studies elsewhere it has been established the various deformation mechanisms producing cataclastic bands in analogue rock types are cause to different internal types of fault fabric and variations in pore throat size and distribution. This will in turn cause significant variations in petrophysical rock properties such as permeability and injection threshold pressure, which are key parameters into the prediction of membrane seal behaviour.

Entry pressure data recorded from Rotliegend (cataclastic) fractures contained within sandstones is difficult to reconcile with AFPD's based on measured well pressure data. This leads to the conclusion that indeed the selected SGR-based algorithms should not indeed be used under conditions where shale material is absent and cataclastic bands the primary type of deformation.

Uncertainties and sensitivities (precision/accuracy) of data and transformations

It has been demonstrated that many deformation bands show reductions in permeability (e.g. Tueckmantel et al., 2010, Shipton et al., 2002), some by as much as several orders of magnitude (Fossen et al., 2007). In single and multi-phase fluid systems other factors likely play an important role as well, but nevertheless host rock and fault permeability appear to be the most important parameters with a practical effect on across-fault fluid flow. As a consequence, many industry workflows for estimating fluid flow properties of faults are based on empirical relationships between (fault) permeability and other parameters such as clay content, porosity or permeability of the host rock. Before accepting an estimate of the fault permeability and fluid flow properties, however, one should be aware of the level of accuracy and precision with respect to the input and output parameters of the various empirical functions used for estimating those fluid flow properties.

In a rather simple workflow such as described by Sperrevik et al (2002), many different conditions may already influence the level of sensitivity and/or uncertainty (or accuracy and precision) of permeability measurements and estimates. These conditions may be related to (and not necessarily restricted to) for example 1) in-situ, small-scale natural variations of (relative) permeability (including the variability of the permeability within fault zones and deformation bands, impact of clay content, relative permeability in presence of multi-phase fluid conditions, in-situ temperature and stress, etc.), 2) conditions of laboratory measurements and their corrections: stress and temperature, type of infiltration fluid, sample integrity, clay content, etc., and 3) the correction and transformation of measured permeability (such as Klinkenberg correction for slippage of gas along pore walls, corrections for stress release when taking core to surface, scale dependency, estimates based on porosity-permeability functions, etc). Estimates of the levels of accuracy and precision of parameters influencing permeability measurements and predictions, may reach to a cumulative absolute order of magnitude on a logarithmic scale of circa 10-15 times hence should be treated with significant care. Other uncertainties and lack of precision are associated with the amount of seismic vertical and horizontal resolution, fault throw, stratigraphic and sedimentary anisotropy and discontinuity, as we as fault activity and its timing.

A sensitivity analysis has been carried out on the two transformations used here to identify which input parameters are cause to uncertainty variations in modelled injection threshold pressure (Sperrevik, 2002) or AFPD (Bretan, 2003). In Bretan's function the uncertainty of AFPD under average Rotliegend reservoir conditions of burial depth (3500m), average Vf (0.1) or SGR (10%) is defined primarily by uncertainty of the estimated SGR. Uncertainty of the injection threshold pressure in Sperrevik's function is primarily dominated by uncertainty in the estimates of the maximum burial depth (77%) and the burial depth at which structural deformation occurred (21%), followed by uncertainty in the surface tension of the gas/water system at reservoir conditions (1%), and shale volume estimates (1%). For the latter it means that surface tension data and shale volume estimates do not contribute significantly to variations in the outcomes.

There are several Rotliegend fields in the Southern Permian Basin in which across-fault variations in reservoir pressure and Free Water Level depths have been observed at (close to) virgin conditions. These AFPDs can be explained by the presence of a semi-permeable fault between wells and/or field compartments acting as a valve. Under certain conditions, small pressure differences between wells measured after the field has been taken into production do not necessarily reflect depletion, but may still be interpreted as a result of membrane sealing either pre-production over geological time, syn-production, or a combination of all of the above.

Two case studies of membrane sealing in fields with Permian Upper Rotliegend reservoir have been carried out and results presented here to validate two selected empirical SGR based functions predicting capillary entry pressures and therefore AFPDS at virgin (pre-production) conditions. It appears that, within an uncertainty range, both functions tested (Sperrevik (2002) and Bretan (2003) plausibly predict expected capillary entry pressures in low N/G reservoir intervals, although some under-/overestimates are observed in relation to maximum burial depth over geological time.

In both case studies performed there were some indications that the AFPD was different measured on a geological time scale at virgin conditions (0-15 bar) against measured on a production time scale (100-200 bar). These observations will require much more evaluation to understand better the dynamic behaviour of the host rock and faults in terms of permeability and capillary entry pressure as a function of (production) time.

The case studies presented here and in the literature have demonstrated the occurrence of fault seal in the high N/G reservoir rocks of the Dutch Rotliegend. There are no published workflows for predicting fault seal over geological time in these lithologies and only a small number of SGR based approaches are available in key industry software. This paper aims to highlight a clear lack in knowledge and act as a call to arms for academics and industry to develop, test and or publish more data to refine and improve tools for faults in high N/G host rock. The approach taken in this paper should ideally be applied across multiple faults, and data pooled from multiple sites to robustly test the hypothesis suggested from these two case studies (Lunn et al., 2008).

Although SGR is usually not recommended for high N/G host rocks that is not necessarily true for SGR- based transforms. Figure 12 shows the permeability and entry pressure dataset from Sperrevik et al. (2002). Most of the data is for rocks with low clay content (0-30%), and the it contains multiple cataclasites. It shows that cataclastic fault rocks may have permeabilities ranging from $1*10^{-4}$ to $1*10^{2}$ mD and Hg-Air threshold pressures of 5-3000psi. Sperrevik reduces the uncertainty somewhat by including burial depth as a parameter, but this still leaves uncertainties of 2-5 orders of magnitude for permeability and up to 2 orders of magnitude for threshold pressure. None of the transforms incorporate this uncertainty, but they return values near the centres of these ranges. Predictions by the selected SGR-based transforms therefore tend to produce reasonable first estimates for faults in high N/G rocks, albeit hampered by several orders of magnitude uncertainty. There is strong potential to develop workflows optimized for fault sealing in rocks with high N/G and this would benefit from more subsurface data released to the public, such as production flow and pressure data, gas composition data, special core analysis data, etc. The above will require multivariate analysis of existing datasets and outcrop studies to derive predictive parameters to minimize the uncertainty in the prediction.

Acknowledgements

The authors wish to acknowledge permission from EBN to publish this paper. Opinions expressed within this paper do not necessarily reflect EBN’s opinions. We thank Neptune Energy Netherlands and partners for sharing data and information of the L12b-C field, and meaningful discussions with them. Further we would like to thank Total E&P Nederland, NAM and partners for providing petrophysical core analysis data of fault samples taken from Rotliegend core from wells across Dutch on- and offshore. The contribution by Yannick Kremer is funded through NERC grant NE/N015908/1.

Abbreviations

AFPD Across Fault Pressure Difference

FWL Free Water Level

GWC Gas Water Contact
N/G Net over Gross ratio
NLOG Netherlands Oil and Gas
RFT Repeated Formation Test
SGR Shale Gouge Ratio
TD Termination or Total Depth
TVD True Vertical Depth
TVDSS True Vertical Depth below Sea-level

References

Adams, S. (2016). *Saturation-height modelling for reservoir description.* Auckland: The Petrophysicist Ltd.

Adrichem Boogaert, H. v., & Kouwe, W. (1993-1997). *Stratigraphic Nomenclature of The Netherlands* (Vol. 50). Mededelingen Rijks Geologische Dienst.

Allan, U. (1989). Model for hydrocarbon migration and entrapment within faulted structures. *American Association of Petroleum Geologists Bulletin*, 387-411.

Antonellini, M., Aydin, A. & Pollard, D.D. (1994). Microstructure of deformation bands in porous sandstones at Arches national Park, Utah. *Journal of Structural Geology*, vol 16, no 7, 941-995.

Aydin, A. (1978). Small faults formed as deformation bands in sandstone. *Pure and Applied Geophysics, 116*, 913-930.

Barr, D. (2007). Conductive faults and sealing fractures in the West Sole gas fields, southern North Sea. In S. Jolley, D. Barr, J. Walsh, & R. Knipe, *Structurally Complex reservoirs* (Vol. Special Publications 347, pp. 431- 455). London: The Geological Society of London.

Belt, F. v. (2007). An intra-basinal mechanism explaning marine-evaporitic cyclicity controlled by sulphate platform progradation and isostatic correction. In F. v. Belt, *Sedimentary cycles in coal and evaporite basinns and the reconstruction of Palaeozoic climate* (Vol. 21). Utrecht: Mededelingen van de Faculteit Geowetenschappen Universiteit Utrecht.

Bretan, P. (2017). Trap Analysis: an automated approach for deriving column height predictions in fault-bounded traps. *Petroleum Geoscience, 23*, 56-69.

Bretan, P., Yielding, G., & Jones, H. (2003). Using calibrated shale gouge ratio to estimate column heights. *American Association of Petroleum Geologists Bulletin, 87*, 397-413.

Busch, B., Winkler, R., Osivandi, K., Nover, G., Amann-Hildebrand, A., & Hilgers, C. (2015). Evolution of small-scale flow barriers in German Rotliegend siliciclastics. In P.J. Armitage, A.R. Butcher, J.M. Churchill, A.E. Csoma, C. Hollis, R. Lander, J.E. Omma and R.H. Worden, *Reservoir Quality of Clastic and Carbonate Rocks: Analysis, Modelling and Prediction* (Vol. 435). London: The Geological Society.

Centrica. (2016). *Ensign, Unravelling the Enigma.* Unpublished report.

Chen, P. (2015). *Fault reactivation analysis of the Cleaver Bank High based on 3D seismic data.* Utrecht University. MSc thesis report.

Corona, F. (2005). Fault trap analysis of the Permian Rotliegend gas play, Lauwerszee Trough, NE Netherlands. In A. Doré, & B. Vining, *Petroleum Geology: North-West Europe and Global Perspectives. Proceedings of the 6th Petroleum Geology Conference* (pp. 327-335). London: The Geological Society.

Courtier, J., & Riches, H. (2003). The V-Fields, Blocks 49/16, 49/21, 48/20a, 48/25b, UK North Sea. In J. Gluyas, & H. Hichens (Eds.), *United Kingdom Oil and Gas Fields Commemorative Millenium Volume*. Geological Society Memoirs 20, pp. 861-870). London: The Geological Society.

Crouch, S., Baumgartner, W., Houllebergh s, E., & Walzebuck, J. (1996). Development of a tight gas reservoir by a multi fracced horizontal well: Ameland-204, the Netherlands. In H. Rondeel, D. Batjes, & W. Nieuwenhuijs, *Geology of Gas and Oil Under the Netherlands* (pp. 93-102). Dordrecht: Royal Geological and Mining Society of the Netherlands, Kluwer Academic Publishers.

Darnet, M., Brain, J., & Loevezijn, P. v. (2015). Unlocking 4D seismic technology to maximize recovery from the pre-salt Rotliegend gas fields of the Southern North Sea. *8th Petroleum Geology of Northwest Europe Conference.* London: The Geological Society.

Dekeyser, D. (1990). *The impact of 3D on the structural interpretation of the Barque and Clipper fields.* Proprietary report Shell UK.

EBN. (2017). *Focus on Energy.* Annual Report EBN

Farmer, R., & Hillier, A. (1991). The Barque Field, Blocks 48/13a, 48/14, UK North Sea. In I. Abbotts, *United Kingdom Oil and gas Fields, 25 Years Commemorative Volume* (pp. 395-400). London: The Geological Society.

Fisher, Q. (2006). *Impact of faults on fluid flow in the Slochteren, onshore and offshore Netherlands.* Rock Deformation Research Ltd. Proprietary report for NAM.

Fisher, Q. (2015). *Faultprop*. Proprietary report for EBN.

Fisher, Q., & Jolley, S. (2007). Treatment of faults in production simulation models. In S. Jolley, D. Barr, J. Walsh, & R. Knipe, *Structurally Complex reservoirs* (Vol. Special Publications 347, pp. 219-233). London: The Geological Society.

Fisher, Q., & Knipe, R. (1998). Fault sealing processes in silliciclastic sediments. In G. Jones, Q. Fisher, & R. Knipe, *Faulting, Fault Sealing and Fluid Flow in Hydrocarbon Reservoirs* (Vol. Special Publ 147, pp. 117-134). London: The Geological Society.

Fisher, Q., Phillips, G., Li, A., & Condliffe, D. (2005). *Petrophysical Properties of Fault Rocks Slochteren Sandstone, offshore and onshore Netherlands.* Rock Deformation Research Ltd. Leeds: Proprietary report for Total.

Fossen, H., Schultz, R., Shipton, Z., & Mair, K. (2007). Deformation bands in sandstone: a review. *Journal of the Geological Society, 164*, 755-769.

Freeman, S., Harris, S., & Knipe, R. (2010). Cross-fault sealing, baffling and fluid flow in 3D geological models: tools for analysis, visualization and interpretation. In S. Jolley, Q. Fisher, R. Ainsworth, P. Vrolijk, & S. Delisle, *Reservoir Compartmentalization* (Vol. 347, pp. 257-282). London: Geological Society Special Publications.

Frikken, H. (1996). CBIL logs: vital for evaluating disappointing well and reservoir performance. In H. Rondeel,

D. Batjes, & W. Nieuwenhuijs, *Geology of Gas and Oil under the Netherlands* (pp. 103-114). Dordrecht: Royal Geological and Mining Society of the Netherlands, Kluwer Academic Publishers.

Gast, R.; Dusar, M.; Breitkreuz, C.; Gaupp, R.; Schneider, J.W.; Stemmerik, L.; Geluk, M.C.; Geißler, M.; Kiersnowski, H.; Glennie, K.; Kabel, S. & Jones, N. (2010). Rotliegend. In H. Doornenbal, & A. Stevenson (Eds.), *Petroleum Geological Atlas of the Southern Permian Basin Area* (pp. 101-121). Houten: EAGE Publications.

Geiss, B. (2008). Late Charge problems in the K5 area. Utrecht. Proprietary report.

Geiss, B., Kremer, Y., Koppen, J. v., & Bertotti, G. (2009). Field compartmentalisation by subtle transfer faulting an example from blocks K4/K5 offshore Netherlands. *7th Conference and Technical Exhibition.* Amsterdam: European Association of Geoscientists and Engineers.

George, G., & Berry, J. (1997). Permian (Upper Rotliegend) synsedimentary tectonics, basin development and palaeogeography of the southern North Sea. In K. Ziegler, P. Turner, & S. Daines (Eds.), *Petroleum Geology of the Southern North Sea: Future Potential* (Vol. 123, pp. 31-61). London: Geological Society Special Publications.

Gras, R., Neale, R., Rossebø, O., & Verkuil, E. (2016). Fault Seal in the Upper Slochteren (Rotliegend), case study from the Gillian gas field, Block L11c, Netherlands Offshore. *EAGE Extended Abstract.* Vienna: EAGE.

Hillier, A. (2003). The Leman Field, Blocks 49/26, 49/27, 49/28, 53/1, 53/2, UK North Sea. In J. Gluyas, & H. Hitchens (Eds.), *United Kingdom Oil and Gas Fields Commemorative Millenium Volume* (Geological Society Memoirs 20, pp. 761-770). London: The Geological Society.

Hillier, A., & Williams, B. (1991). The Leman Field, Blocks 49/26, 49/27, 49/28, 53/1, 53/2, UK North Sea. In I. Abbotts, *United Kingdom Oil and gas Fields, 25 Years Commemorative Volume* (pp. 451-458). London: The Geological Society.

Hulten, F. v. (2010). Geological factors effecting compartmentalization of Rotliegend gas fields in the Netherlands. In S. Jolley, Q. Fisher, R. Ainsworth, P. Vrolijk, & S. Delisle, *Reservoir Compartmentailzation* (Special Publications 347, pp. 301-315). London: The Geological Society.

Hulten, v. F. (1996). Compartmentalized gas reservoirs of the Netherlands. *American Association of Petroleum Geologists /EAGE Research Symposium Compartmentalized Reservoirs: Their Detection, Characterization and Management.* Tulsa: American Association of Petroleum Geologists.

Jager, J. d., & Geluk, M. (2007). Petroleum Geology. In T. Wong, D. Batjes, & J. d. Jager (Eds.), *Geology of the Netherlands* (pp. 241-264). Royal Netherlands Academy of Arts and Sciences.

Jolley, S., Dijk, H., Lamens, J., Fisher, Q., Manzocchi, T., Eikmans, H., & Huang, Y. (2007). Faulting and fault sealing in production simulation models: Brent Province, northern North Sea. *Petroleum Geoscience, 13*, 321-340.

Knipe, R. (1997). Juxtaposition and Seal Diagrams to Help Analyze Fault Seals in Hydrocarbon Reservoirs. *American Association of Petroleum Geologists Bulletin, 81*(2), 187-195.

Knipe, R.J., Q.J. Fisher, M.B. Clennel, A.B. Farmer, B. Kidd, E. McAllister, J.R. Porter, & A.A. White (1997). Fault seal analysis: successful methodologies, applications and future directions. In P. Moller-Pederson, & A. Koestler, *Hydrocarbon seals: importance for exploration and production* (Norwegian Petroleum Society

Special Publication 7, pp. 15-40). Elsevier.

Kremer, Y., Shipton, Z., Lunn, R., Wibberley, C., & Sosio de Rosa, S. (In press). What's inside a fault? Architecture and composition of faults in sand-shale-silt sequences. *American Association of Petroleum Geologists Bulletin*.

Lander, R.H. & Laubach, S.E. (2014). Cementation in fractured sandstones Insights into rates of fracture growth and sealing from a model for quartz. Geological Society of America Bulletin, vol 127, no 3-4.

Leveille, G.P., R. Knipe, C. More, D. Ellis, G. Dudley, G. Jones, Q.J. Fisher, & G. Allinson (1997). Compartmentalization of Rotliegend gas reservoirs by sealing faults, Jupiter Fields area, southern North Sea. In K. Ziegler, P. Turner, & S. Daines, *Petroleum Geology of the Southern North Sea: Future Potential* (pp. 87-104). London: Geological Society Special Publications.

Ligtenberg, H., Okkerman, J., & Keijzer, M. d. (2011). Fractures in the Dutch Rotliegend - An overview. In J. Grotsch, & R. Gaupp, *The Permian Rotliegend of the Netherlands* (Vol. 98, pp. 229-244). SEPM Special Publication.

Lindsay, N., Murphy, F., Walsh, J., & Watterson, J. (1993). Outcrop studies of shale smears on fault surfaces. In S. Flint, & A. Bryant, *The Geological Modelling of Hydrocarbon Reservoirs and Outcrop* (Special Publications 15, pp. 113-123). International Association of Sedimentology.

Lunn, R., Shipton, Z., & Brigth, A. (2008). How can we improve estimates of bulk fault zone hydraulic properties? *Geological Society London Special Publications, 299*, 231.

Manzocchi, T., Walsh, J., Nell, P., & Yielding, G. (1999). Fault transmissibility multipliers for simulation models. *Petroleum Geoscience, 5*, 53-63.

Mauthe, G. (2003). Sealing Faults Due to Cataclasis in Rotliegend Sandstones (Lower Permian) of NW-Germany. *Erdöl Erdgas Kohle, 119*(1), 12-17.

McCrone, C., Gainski, M., & Lumsden, P. (2003). The Indefatigable Field, Blocks 49/18, 49/19, 49/23, 49/24, UK North Sea. In J. Gluyas, & H. Hichens (Eds.), *United Kingdom Oil and Gas Fields Commemorative Millenium Volume* (Geological Society Memoirs 20, pp. 741-747). London: The Geological Society.

Molen, I. v., Zijlstra, E., Okkerman, J., & Reemst, P. (2003). Compartmentalisation in Rotliegend gas fields, examples from offshore and onshore The Netherlands. *Fault and Top Seals: What do we know and where do we go? Paper-28*, pp. 1-3. Houten: European Association of Geoscientists and Engineers.

Nelskamp, S., Abdul Fattah, R., Verweij, J., & Witmans, N. (2014). An Overview of Basin Modeling in the Netherlands - New Results and Applications. *76th EAGE Conference & Exhibition 2014.* Amsterdam: EAGE.

Ojik, K. v., Böhm, A., Cremer, H., Geluk, M., Jong, M. d., Mijnlieff, H., & Nio, S. (2011). The rationale for an integrated stratigraphic framework of the Upper Rotliegend II depositional system in the Netherlands. In *The Permian Rotliegend in the Netherlands* (Vol. 98, pp. 37-48). SEPM Special Publication.

Oudmayer, B., & Jager, J. d. (1993). Fault reactivation and oblique-slip in the Southern North Sea. In J. Parker (Ed.), *Petroleum Geology of Northwest Europe: Proceedings of the 4th Conference* (pp. 1281-1290). London: The Geological Society.

Pearson, J., Young, R., & Smith, A. (1991). The Indefatigable Field, Blocks 49/18, 49/19, 49/23, 49/24, UK North

Sea. In I. Abbotts, *United Kingdom Oil and Gas Fields, 25 Years Commemorative Volume* (pp. 443-450). London: The Geological Society.

Pharaoh, T., M. Dusar,, M.C. Geluk, F. Kockel, C. Krawczyk, P. Krzywiec, M. Scheck-Wenderoth, H. Thybo, O. Vejbæk, & J.D. van Wees (2010). Tectonic evolution. In H. Doornenbal, & A. Stevenson (Eds.), *Petroleum Geological Atlas of the Southern Permian Basin Area* (pp. 25-57). Houten: EAGE Publications.

Sarginson, M. (2003). The Barque Field, Blocks 48/13aa, 48/14, UK North Sea. In J. Gluyas, & H. Hichens (Eds.), *United Kingdom Oil and Gas Fields Commemorative Millenium Volume* (Geological Society Memoirs 20, pp. 663-670). London: The Geological Society.

Schowalter, T. (1979). Mechanics of secondary hydrocarbon migration and entrapment. *American Association of Petroleum Geologists Bulletin, 63*, 723-760.

Schroot, B., & Haan, H. d. (2003). An improved regional structural model of the Upper Carboniferous of the Cleaver Bank High based on 3D seismic interpretation. In D. Nieuwland (Ed.), *New Insights into Structural Interpretation and Modelling* (Vol. 212, pp. 23-37). London: Geological Society Special Publications.

Shipton, Z. & Cowie, P.A. (2001). Damage zone and slip-surface evolution over µm to km scales in high-porosity Navajo sandstone, Utah, *J. Struct. Geol*., 23, 1825-1844.

Shipton, Z. K., & Cowie, P.A. (2003). A conceptual model for the origin of fault damage zone structures in high-porosity sandstone, *J. Struct. Geol.*, 25, 333-345.

Shipton, Z., Evans, J., Robeson, K., Forster, C., & Snelgrove, S. (2002). Structural heterogeneity and permeability in faulted eolian sandstone: Implications for subsurface modeling of faults. *American Association of Petroleum Geologists Bulletin, 86*, 863-883.

Shipton, Z., Soden, A., Kirkpatrick, J., Bright, A., & Lunn, R. (2006). How thick is a fault? Fault displacement-thickness scaling revisited. In R. Abercrombie (Ed.), *Earthquakes: Radiated Energy and the Physics of Faulting* (pp. 193-198). AGU.

Sperrevik, S., Gillespie, P., Fisher, Q., Halvorsen, T., & Knipe, R. (2002). Empirical estimation of fault rock properties. In A. Koestler, & R. Hunsdale, *Hydrocarbon Seal Quantification* (Vol. 11, pp. 109-125). Norwegian Petroleum Society Special Publications.

Tueckmantel, C., Fisher, Q., Knipe, R., Lickorish, H., & Khalil, S. (2010). Fault seal prediction of seismic-scale normal faults in porous sandstone: A case study from the eastern Gulf of Suez rift, Egypt. *Marine and Petroleum Geology, 27*, 334-350.

Underschultz, J. (2007). Hydrodynamics and membrane seal capacity. *Geofluids, 7*, 148-158.

Vendeville, B., & Jackson, M. (1992). The rise of diapirs during thin-skinned extension. *Marine and Petroleum Geology, 9*(4), 331-354.

Walderhaug, O. (1996). Kinetic modeling of quartz cementation and porosity loss in deeply buried sandstone reservoirs. *American Association of Petroleum Geologists Bulletin, 80*, 731-745.

Weijermans, P., Daniau, G., & Westerhof, D. (2016). Developing Marginal Near-Tight Gas Fields in a Mature Area With Long-Reach Hydraulically Fractured Wells - A Case Study. *SPE Europec featured at 78th*

EAGE Conference and Exhibition. Society of Petroleum Engineers.

Wijhe, D. v., Lutz, M., & Kaasschieter, J. (1980). The Rotliegend in the Netherlands and its gas accumulations. *Geologie en Mijnbouw, 59*(1), 3-24.

Winter, D., & King, B. (1991). The West Sole Field, Block 48/6, UK North Sea. In I. Abbotts, *United Kingdom Oil and gas Fields, 25 Years Commemorative Volume* (pp. 451-458). London: The Geological Society.

Yielding, G. (2002). Shale Gouge Ratio – Calibration by Geohistory. In A. Koestler, & R. Hunsdale, *Hydrocarbon Seal Quantification* (Vol. 11, pp. 1-15). Amsterdam: Norwegian Petroleum Society (NPF) Special Publications.

Yielding, G., Bretan, P., & Freman, B. (2010). Fault seal calibration: a brief review. In S. Jolley, Q. Fisher, R. Ainsworth, P. Vrolijk, & S. Delisle, *Reservoir Compartmentalization* (Vol. Special Publications 347, pp. 243-255). London: The Geological Society of London.

Yielding, G., Freeman, B., & Needham, T. (1997). Quantitative Fault Seal Prediction. *American Association of Petroleum Geologists Bulletin, 81*, 897-917.

Ziegler, P. (1990). *Geological Atlas of Western and Central Europe.* London: Shell Internationale Petroleum Maatschappij BV/The Geological Society of London.

Zijlstra, E., Reemst, P., & Fisher, Q. (2007). Incorporation of fault properties into production simulation models of Permian reservoirs from the southern North Sea. In S. Jolley, D. Barr, J. Walsh, & R. Knipe, *Structurally Complex reservoirs* (Special Publications 347, pp. 295-308). London: The Geological Society.

List of Tables

Table 1: Upper Rotliegend fields from the UK, Dutch and German on- and offshore where membrane seals were identified (level of confidence indicated in column 2).

Table 2: Overview of availability of fault samples from Rotliegend cores for petrophysical core analysis (Fisher, et al., 2005, 2006; Leveille, et al., 1997; Mauthe, 2003)

Table 3: Statistical overview of core analysis data available from samples from wells in the UK and Dutch offshore and Dutch and German onshore areas (Fisher et al, 2005, 2006).

List of figures

Figure 1: Base map of the southern North Sea with overview of fields where membrane seal at Rotliegend reservoir level were identified. Numbers at dots refer to fields in table 1.

Figure 2: Simplified stratigraphic table of the Permian and Carboniferous stratigraphic sequence.

Figure 3: Simplified map of the present-day distribution of sediments of the Upper Rotliegend Group in the central Dutch offshore and north onshore area. Included here are oil and gas discoveries in the Rotliegend, and all released wells which have completely penetrated the Rotliegend. Numbers refer to fields/areas collected in table 1 where membrane seals are identified. The dashed black line represents the 100m isochore contour (thinner towards the South, thicker to the North), the stippled grey lines represent iso-Vshale contours (average Vsh> 0.75 towards the North, East-West stretching belt with average Vsh between 0.25 and 0.75, and average Vsh < 0.25 towards the South), the green filled polygon represents the area where the top of the Rotliegend is buried at present-day depth shallower than 3km, and the yellow filled polygon represents the area where the average porosity is larger than circa 15%.

Figure 4: a) Simplified and conceptual fault map at Base Zechstein seismic reflector showing orientation and spacing of typical fault framework seismically visible at Top Rotliegend level with several generations of fault directions and character, map including position of the L12b-C field. b) Overview of regional tectonic kinematic history in time (horizontal axis) and approximate depth of burial and temperature (at base Rotliegend) at time of deformation (vertical axis). Red arrows represent directions of compressional events, green arrows represent extensional events (modified after Ligtenberget al., 2011).

Figure 5: Illumination of fault pattern distribution in seismic attribute map (gradient) at Top Rotliegend in the K4/K5 area, offshore Netherlands (after Geiss, 2008) showing the presence of pervasive, long NE-SE trending lineaments referred to as ‘ De Keyser’ faults (Dekeyser, 1990).

Figure 6: Pairs of fault rock vs host rock permeability for selected core samples from the Rotliegend in British,

German and Dutch on- and offshore wells (Fisher et al., 2005, 2006; Leveille, et al., 1997; Mauthe, 2003).

Figure 7: Cross plot of host rock clay content versus fault rock permeability of rock samples collected from Rotliegend core (Fisher et al., 2005, 2006). Symbol colour indicative for type of fault rock, symbol size proportional to present day burial depth. Included are several common public transformations between host rock clay content and fault rock permeability (Jolley et al., 2007; Manzocchi et al., 1999; Fisher, 2015; Bretan et al., 2003).

Figure 8: Cross-plot of in-situ (gas/brine system) capillary entry pressures (in bar) vs reconstructed maximum burial depth of fault rock samples from core after (Fisher et al., 2005, 2006). Included are two data-points from fields where Across Fault Pressure Differences (in bar) have been estimated based on well pressure data (see this paper for explanation).

Figure 9: Cross-plot of Hg-Air injection threshold pressures versus clay content of fault rock samples collected from Rotliegend cores. Symbol size proportional to maximum reconstructed burial depth. Modified after Fisher et al. (2005, 2006),. Included are empirical property transformation functions by Fisher (2015), Bretan et al (2003) and Sperrevik et al. (2002).

Figure 10: Conceptual diagram for Rotliegend fault seal: (A) cross section with discontinuous gas phase and different FWL's on both sides of a fault, but at a uniform water pressure gradient, and (B) corresponding pressure-depth plot with uniform hydrostatic pressure gradient for aquifer and different gas pressure gradients for Well A and B, with Pt = threshold pressure equals buoyancy pressure. Modified after Underschultz (2007).

Figure 11: Generalized stratigraphy and GR log from well L12-3 in the L12b-C field. All depth values in meters tvdss. The reservoir sequence has been divided into sub-units based on lithology interpretation. Slochteren A, C, and E sub-units are dominated by silt, the Slochteren B and D sub-units are the main flow-units dominated by sand.

Figure 12: NW-SE cross section over the L12b-C field illustrating the structural compartmentalisation due to faults into a northern, central and southern domain, the position of the 4 wells drilled into the field, and the depth of the FWL across the field based on well observations. The position of the dividing fault between the southern and central domain in relation to well L15-4 is subject to interpretation: based on seismic data several structural framework scenarios can be identified here, putting the well either in the Central or Southern Domain.

Figure 13: Fault juxtaposition triangle diagram based on discrete lithology classification of the L12-3 reservoir sequence into sand, silt and shale juxtaposed against itself at increasing amount of throw.

Figure 14: 3D view from the South towards dividing fault between northern and central domain, with display of juxtaposition property on fault face based on 3 discrete lithology classes (sand, silt, shale) above FWL (horizontal plane). Well sticks of A108A (in front of fault) and L12-3 and A106 (behind the fault) with depth labels (in meters TVD). The fault is almost vertical slightly dipping towards the South, with the foot wall of the fault located in the North (behind the fault face), and the hanging wall in the South (in front of the fault face).

Figure 15: Formation pressure data plot for the L12b-C Field, including: RFT from well L12-3 (1979) in the Northern Domain and well L15-4 (1982) in the Middle/Southern Domain, allowing the interpretation of different Free water Levels on both sides of the dividing fault , and an Across Fault Pressure Difference of circa 4 bar at virgin conditions. In addition, formation pressure data has been acquired in well 108A (2014) in the Middle Domain, at which time the reservoir pressure in the Middle/Southern Domain was decreased with circa 50 bar to circa 285 bara, and in the Northern Domain was decreased due to production to circa 50 bara, allowing the calculation of an Across Fault Pressure Difference of circa 235 bar.

Figure 16: Depth-pressure cross-plot including an estimation of the capillary entry pressure profiles of one of the pillars at the East-West trending bounding fault between the Northern and Central compartment. The depth interval represents the approximate area of self-juxtaposition of the lower reservoir unit B. Entry pressures profiles are based on Bretan et al (2003) (green curve at the left hand side) and Sperrevik et al. (2002) (red curve at the right hand side) including their inherited uncertainty ranges. The vertical black line represents the AFPD measured between wells on either side of the fault, with the hatched area representing the uncertainty range of these AFPD measurements

Figure 17: Schematic overview of field SNS-A.

Figure 18: Generalized stratigraphy and GR log from well WC in the SNS-A field. All depth values in meters tvdss. The Lower Slochteren reservoir sequence has been divided into sub-units Alpha (predominantly sand) and Beta (predominantly shale and silt).

Figure 19: Formation pressure data plot for the SNS-A Field, including: pressure points from well WA in the southern BX block and WB and WC in the Northern BY block and an Across Fault Pressure Difference of circa 4 bar. In addition, formation pressure data has been acquired later after several years of production from the BX block in well WC located in the northern BY block,

Figure 20: Pressure-depth of plot of the bounding fault between SNS-A-BX and -BY compartments showing the vertical distribution of base case capillary entry pressure profiles in the Lower Slochteren Alpha unit for Bretan function (green curve) and Sperrevik function (red curve). The black line (1) represents the AFPD at this bounding fault (with uncertainty range).

List of appendices

Appendix 1: Petrophysical properties of Rotliegend Fault rocks

Field/area	Level of confidence	Supporting evidence	Type of fault seal analysis	Number in basemap	Cou ntry	Reference
Ameland field	Possible	Pressure differences		4	NL	Crouch et al.,1996
Onshore NE Netherlands including Kommerzijl, Ezumazijl & Burum	Most probable	Different FWL's and/or significant pressure differences across faults	Petrophysical analysis of fault rock data ,material balance, dynamic production history matching	6, 7, 8	NL	Corona, 2005; van Hulten, 2010, van der Molen et al., 2003, Zijlstra et al., 2007
Grijpskerk field	Probable	Different FWL's		9	NL	Van Hulten, 2010
K12-A & K12-E fields	Possible	Different FWL's	Structural fault analysis	1, 2	NL	Rijkers, 2008
K15-FG field	Most probable	Pressure differences	Seismic attributes	10	NL	Frikken, 1996; Darnet et al., 2015
K4/K5 blocks	Most probable	Pressure differences	Petrophysical analysis of fault rock data , SGR based transmissibility multipliers feeding into dynamic production history matching	15	NL	Geiss, pers com.; Fisher et al., 2005
L10-4 well	Possible	FWL differences	Structural fault analysis	3	NL	Rijkers, pers comm; van Hulten, 2010
L11-Gillian field	Possible	Pressure differences	Structural fault analysis , seismic attributes	14	NL	Gras, 2016
L12b-C & L15b-A fields	Most probable	FWL and pressure differences	Static pressure analysis, dynamic production history matching	18, 19	NL	Weijermans et al., 2016
L13-FE field	Possible	Pressure decline	Dynamic production	11	NL	Frikken, 1996

Field/area	Level of confidence	Supporting evidence	Type of fault seal analysis	Number in basemap	Country	Reference
			history matching			
Barque Field	Possible	FWL and pressure differences		22	UK	(Farmer & Hillier, 1991), (Sarginson, 2003)
Clipper Field	Possible	FWL and pressure differences		21	UK	(Farmer & Hillier, 1991)
Cobra field	Probable	FWL and pressure differences	SGR based column height predictions	24	UK	(Bretan, 2017) (Murray & Johnson, 2016)
Ensign Field	Possible	FWL and pressure differences		34	UK	(Centrica, 2016)
Indefatigable field	Possible	FWL differences		25	UK	(Pearson, Young, & Smith, 1991), (McCrone, Gainski, & Lumsden, 2003)
Jupiter Fields	Most probable	FWL and pressure differences	Petrophysical analysis of fault rock data	27	UK	(Leveille, et al., 1997)
Leman Field / Anonymous Field A	Probable	Pressure decline	Dynamic production history matching, SGR based capillary entry height model	28	UK	(Hillier & Williams, 1991), (Hillier, 2003) (Zijlstra, Reemst, & Fisher, 2007)
V-Fields (Vanguard, Valiant, Vulcan)	Probable	FWL and pressure differences	Dynamic production history matching	31	UK	(Courtier & Riches, 2003)
West Sole fields (West Sole, Newsham, Hoton)	Probable	FWL and pressure differences	Petrophysical analysis of fault rock data , dynamic production history	32	UK	(Barr, 2007), (Winter & King, 1991)

Field/area	Level of confidence	Supporting evidence	Type of fault seal analysis	Number in basemap	Cou ntry	Reference
			matching			
Schneverdingen Graben area	Probable	FWL and pressure differences	Petrophysical analysis of fault rock data	33	GE	(Mauthe, 2003)
Schneverdingen Graben area (Rotenburg Field?)	Most probable	FWL and pressure differences	Petrophysical analysis of fault rock data fed into dynamic history matching	34	GE	(Busch, et al., 2015)

Table 1: Published examples and case studies of Upper Rotliegend areas/fields from the UK, Dutch and German on- and offshore where fault sealing aspects have been identified (likelihood for presence of fault sealing indicated in column 2 with level of confidence)

Source Fault rock type (Fossen et al, 2007)	Fisher et al (2005)	Leveille et al (1997)	Mauthe et al (2003)
Phyllosilicate band	-	-	-
(Proto) cataclastic band	13	5	21
Cemented band	1	3	-
Combined cataclastic and cemented bands	4	-	--

Table 2: Overview of availability of fault samples from Rotliegend cores for petrophysical core analysis (Fisher, et al., 2005) (Leveille, et al., 1997) (Mauthe, 2003)

Core rock measurement type	Sample from fault or host rock	Number of samples	Minimum	Maximum	Geometric mean	Geometric mean minus 1 µ	Geometric mean plus 1 µ
Permeability in mD	Fault	72	0,00027	1,10	0.008	0.001	0.057
	Host	68	0,00500	1300	2.758	0.14	53.8
Hg injection threshold pressure in bar	Fault	42	2,48211	200,9	13.15	4.24	40.8
	Host	38	0,13790	20,68	0.848	0.28	2.59

Table 3: Statistical overview of core analysis data available from samples from wells in the UK and Dutch offshore and Dutch and German onshore areas ((Fisher, et al., 2005) (Leveille, et al., 1997) (Mauthe, 2003)

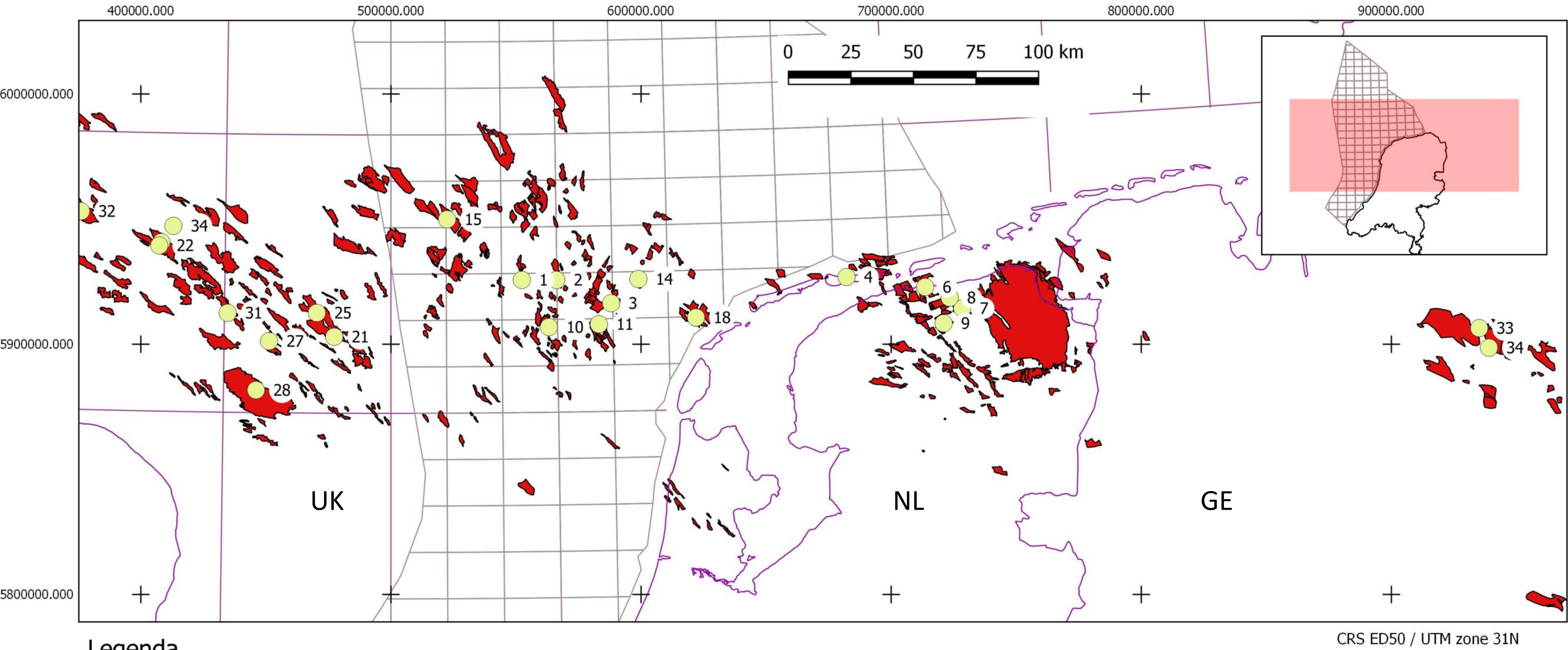

Legenda

Culture

Offshore block boundaries

Dutch onshore territorial boundary

Fault Sealing

Rotliegend fields with membrane seals published

Fields

Gas fields Rotliegend

gas

Figure 1

<table>
<tr><td rowspan="7">(Upper) Permian</td><td rowspan="2">Zechstein Gp (Evaporites)</td><td>Evaporites</td></tr>
<tr><td>Coppershale Mb</td></tr>
<tr><td rowspan="5">Upper Rotliegend Gp</td><td>Ten Boer Mb (Shales)</td></tr>
<tr><td>Upper Slochteren Mb (Sandstones)</td></tr>
<tr><td>Ameland Mb (Shales)</td></tr>
<tr><td>Lower Slochteren Mb (Sandstones)</td></tr>
<tr></tr>
<tr><td colspan="3">Base Permian Unconformity (BPU)</td></tr>
<tr><td>Carbon-iferous</td><td colspan="2">Limburg Gp (Sand-shale-coal)</td></tr>
</table>

Figure 2

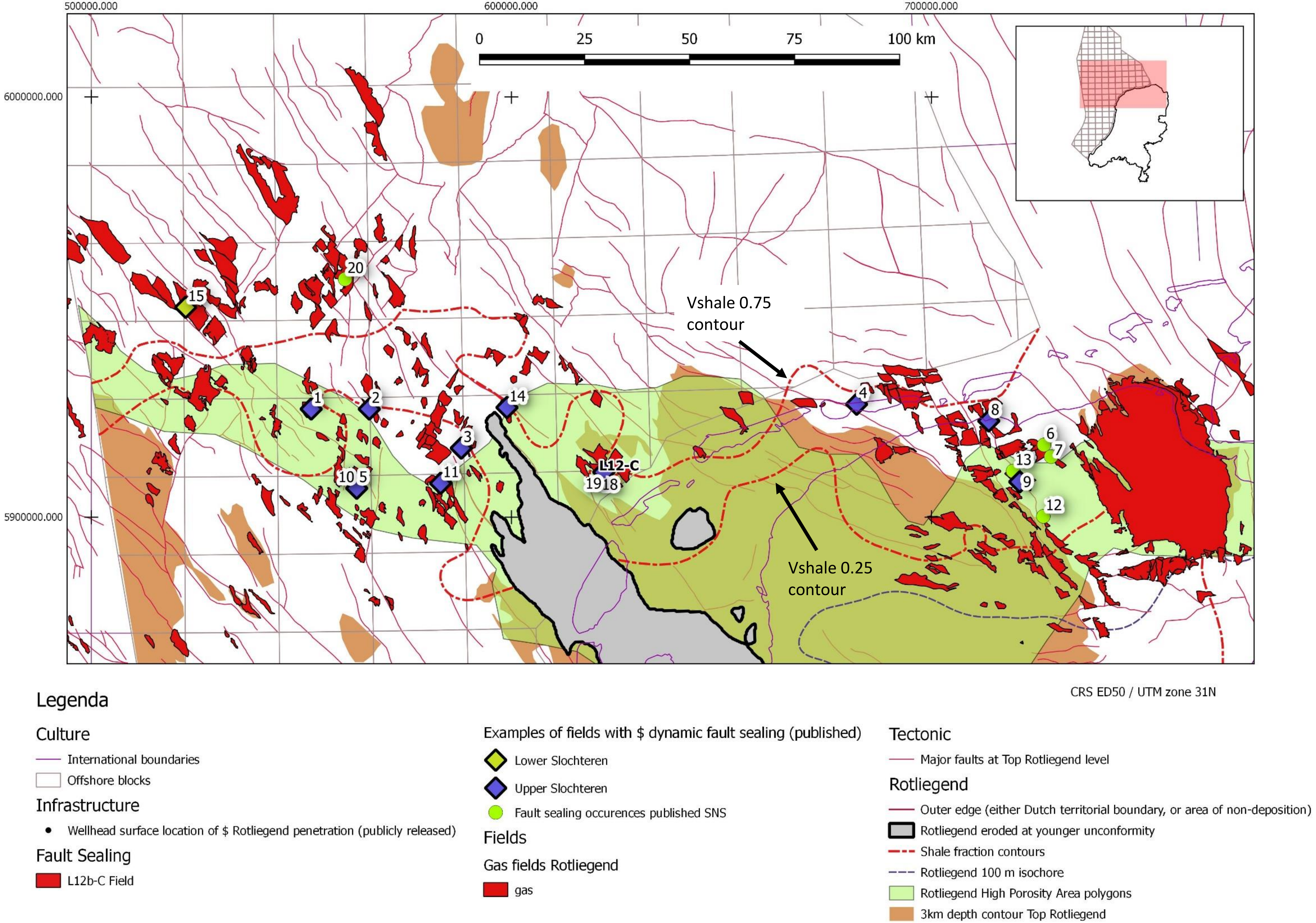
500000.000
600000.000
700000.000
6000000.000
5900000.000
0
25
50
75
100 km
20
15
Vshale 0.75
contour
1
2
14
4
8
3
6
7
13
L12-C
10 5
11
19 18
9
12
Vshale 0.25
contour
CRS ED50 / UTM zone 31N
Legenda
Culture
International boundaries
Offshore blocks
Infrastructure
Wellhead surface location of $ Rotliegend penetration (publicly released)
Fault Sealing
L12b-C Field
Examples of fields with $ dynamic fault sealing (published)
Lower Slochteren
Upper Slochteren
Fault sealing occurences published SNS
Fields
Gas fields Rotliegend
gas
Tectonic
Major faults at Top Rotliegend level
Rotliegend
Outer edge (either Dutch territorial boundary, or area of non-deposition)
Rotliegend eroded at younger unconformity
Shale fraction contours
Rotliegend 100 m isochore
Rotliegend High Porosity Area polygons
3km depth contour Top Rotliegend

Figure 3

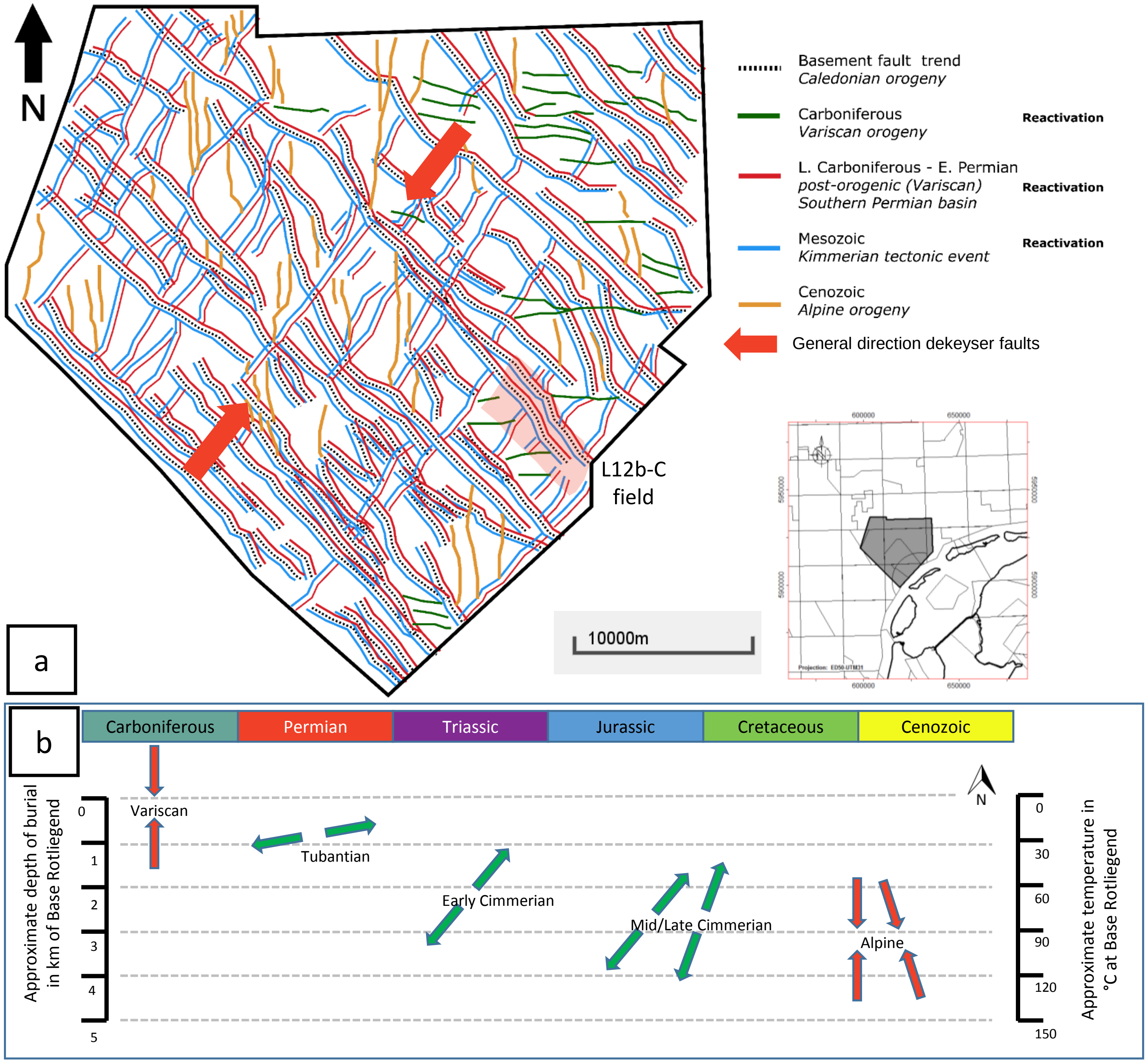
N
Basement fault trend
Caledonian orogeny
Carboniferous
Variscan orogeny
Reactivation
L. Carboniferous - E. Permian
post-orogenic (Variscan)
Southern Permian basin
Reactivation
Mesozoic
Kimmerian tectonic event
Reactivation
Cenozoic
Alpine orogeny
General direction dekeyser faults
L12b-C
field
10000m
a
b
Carboniferous
Permian
Triassic
Jurassic
Cretaceous
Cenozoic
Variscan
Tubantian
Early Cimmerian
Mid/Late Cimmerian
Alpine
N
Approximate depth of burial in km of Base Rotliegend
0
1
2
3
4
5
Approximate temperature in °C at Base Rotliegend
0
30
60
90
120
150

Figure 4

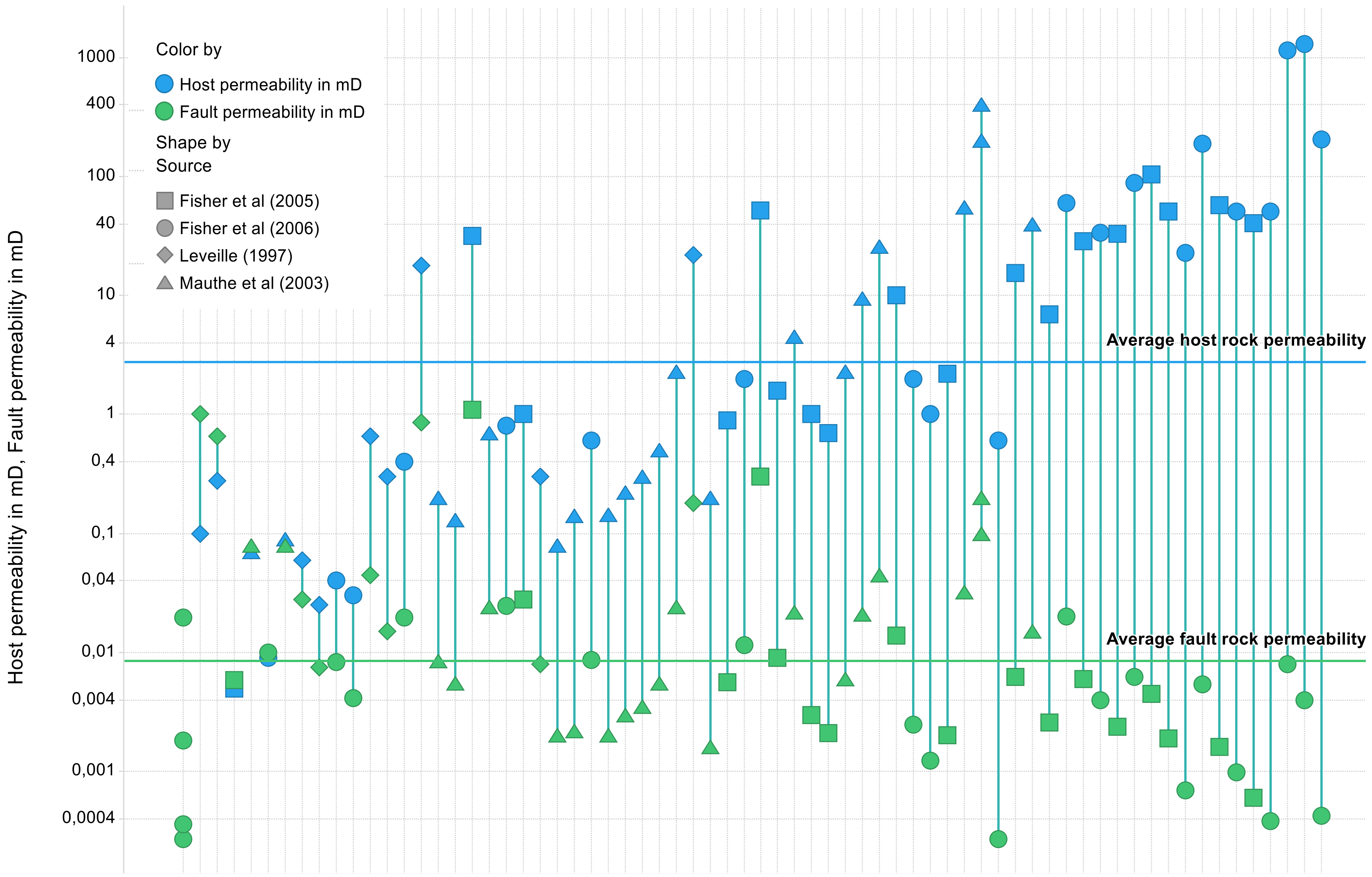
Host permeability in mD, Fault permeability in mD
1000
400
100
40
10
4
1
0,4
0,1
0,04
0,01
0,004
0,001
0,0004
Color by
Host permeability in mD
Fault permeability in mD
Shape by
Source
Fisher et al (2005)
Fisher et al (2006)
Leveille (1997)
Mauthe et al (2003)
Average host rock permeability
Average fault rock permeability

Figure 6

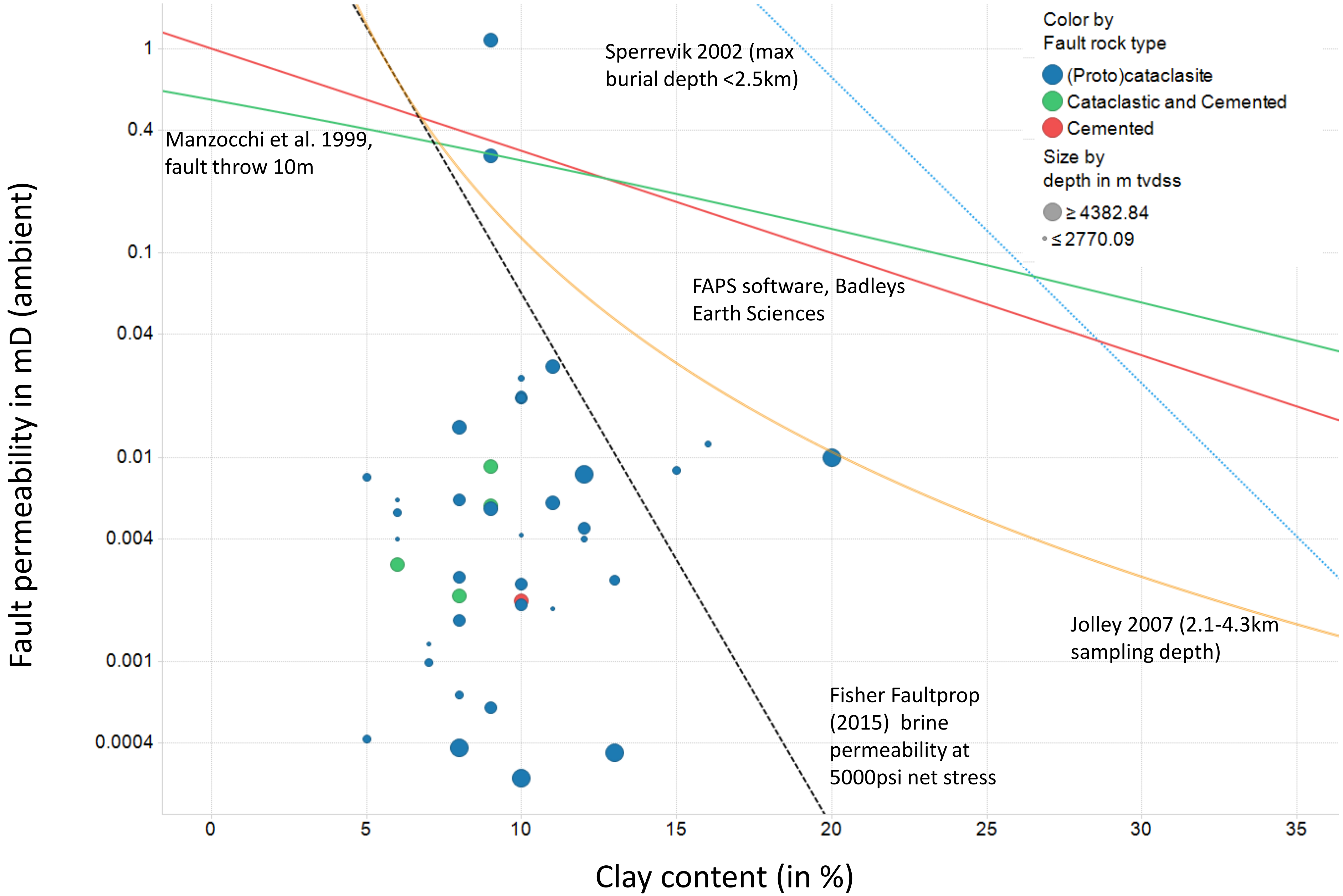
Fault permeability in mD (ambient)
1
0.4
0.1
0.04
0.01
0.004
0.001
0.0004
Clay content (in %)
0
5
10
15
20
25
30
35
Sperrevik 2002 (max burial depth <2.5km)
Manzocchi et al. 1999, fault throw 10m
FAPS software, Badleys Earth Sciences
Jolley 2007 (2.1-4.3km sampling depth)
Fisher Faultprop (2015) brine permeability at 5000psi net stress
Color by
Fault rock type
(Proto)cataclasite
Cataclastic and Cemented
Cemented
Size by
depth in m tvdss
≥ 4382.84
≤ 2770.09

Figure 7

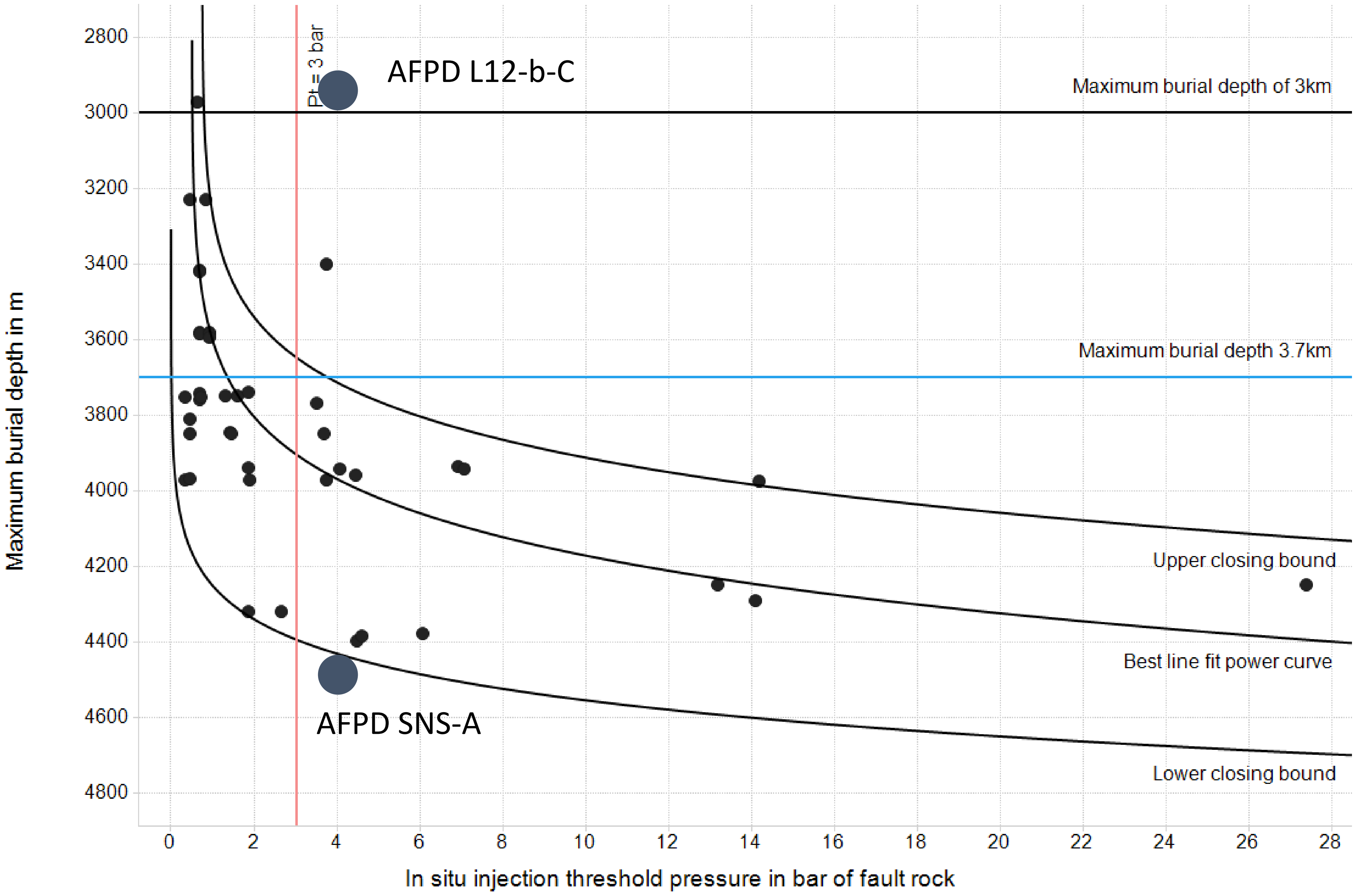

Maximum burial depth in m
2800
3000
3200
3400
3600
3800
4000
4200
4400
4600
4800
0
2
4
6
8
10
12
14
16
18
20
22
24
26
28
In situ injection threshold pressure in bar of fault rock
Pt = 3 bar
AFPD L12-b-C
Maximum burial depth of 3km
Maximum burial depth 3.7km
Upper closing bound
Best line fit power curve
AFPD SNS-A
Lower closing bound

Figure 8

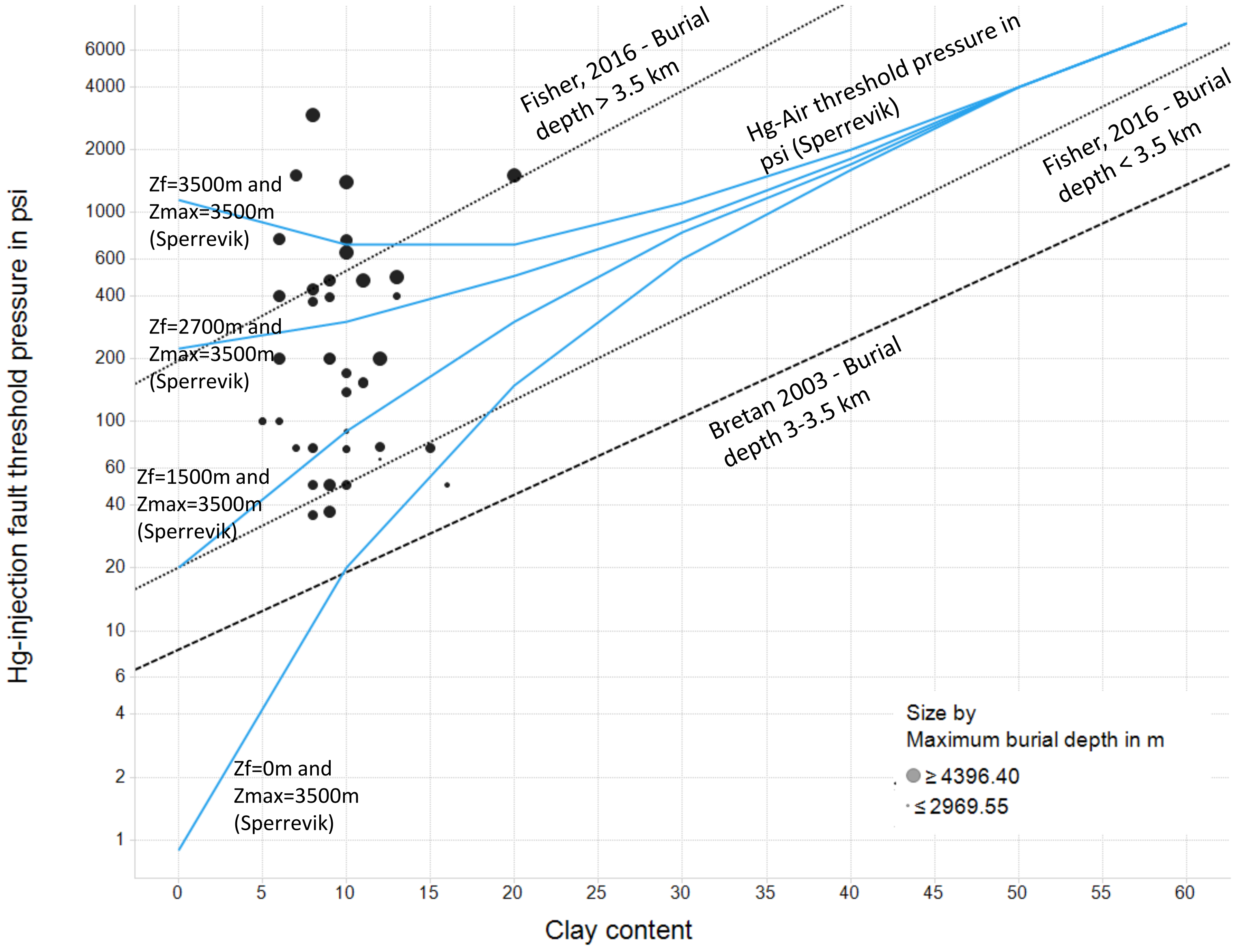

Fisher, 2016 - Burial depth > 3.5 km
Hg-Air threshold pressure in psi (Sperrevik)
Fisher, 2016 - Burial depth < 3.5 km
Bretan 2003 - Burial depth 3-3.5 km
Zf=3500m and Zmax=3500m (Sperrevik)
Zf=2700m and Zmax=3500m (Sperrevik)
Zf=1500m and Zmax=3500m (Sperrevik)
Zf=0m and Zmax=3500m (Sperrevik)
Size by Maximum burial depth in m
≥ 4396.40
≤ 2969.55
Hg-injection fault threshold pressure in psi
Clay content

Figure 9

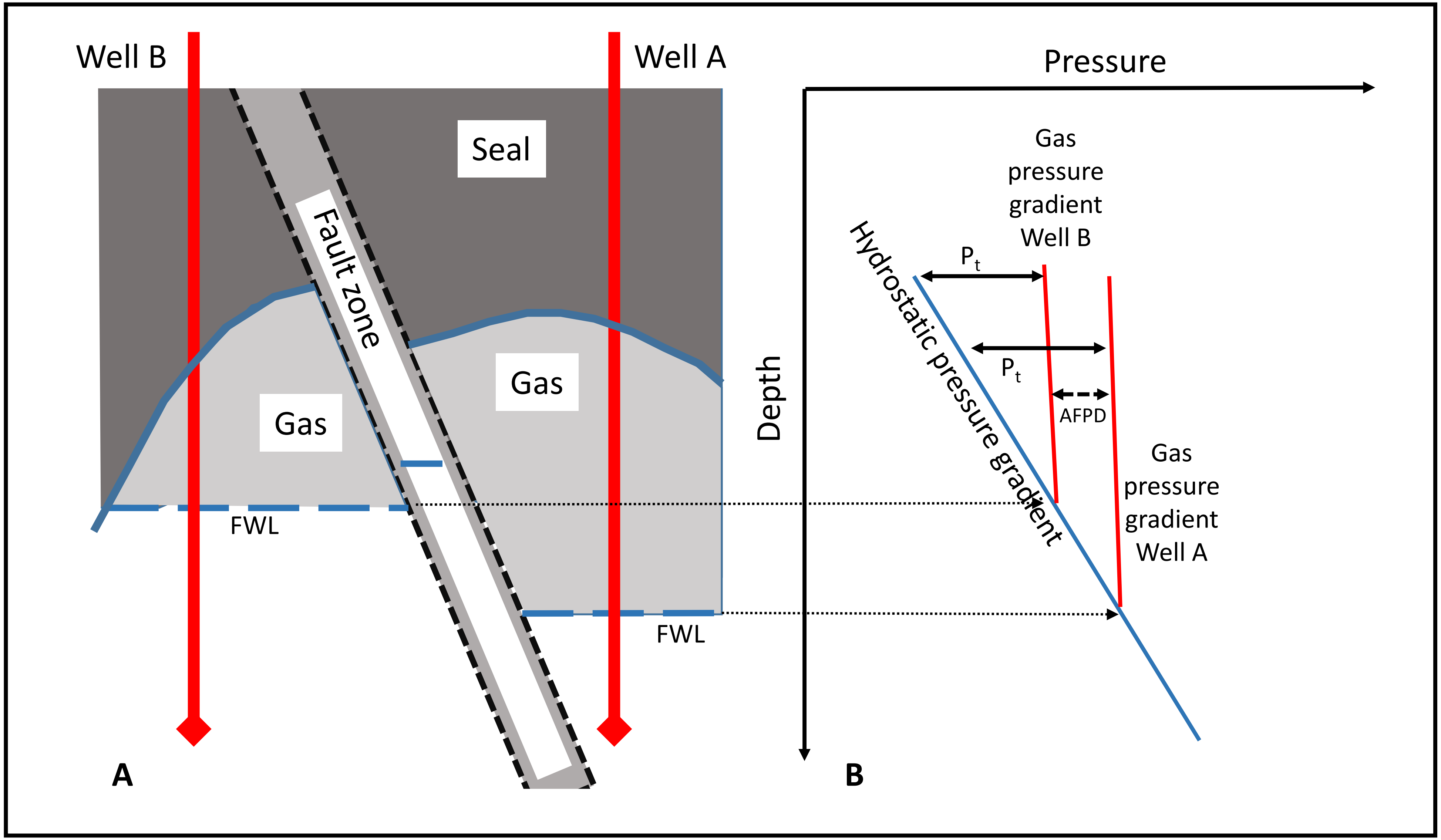
Well B
Well A
Seal
Fault zone
Gas
Gas
FWL
FWL
A
Pressure
Depth
Gas pressure gradient Well B
Hydrostatic pressure gradient
P_t
P_t
AFPD
Gas pressure gradient Well A
B

Figure 10

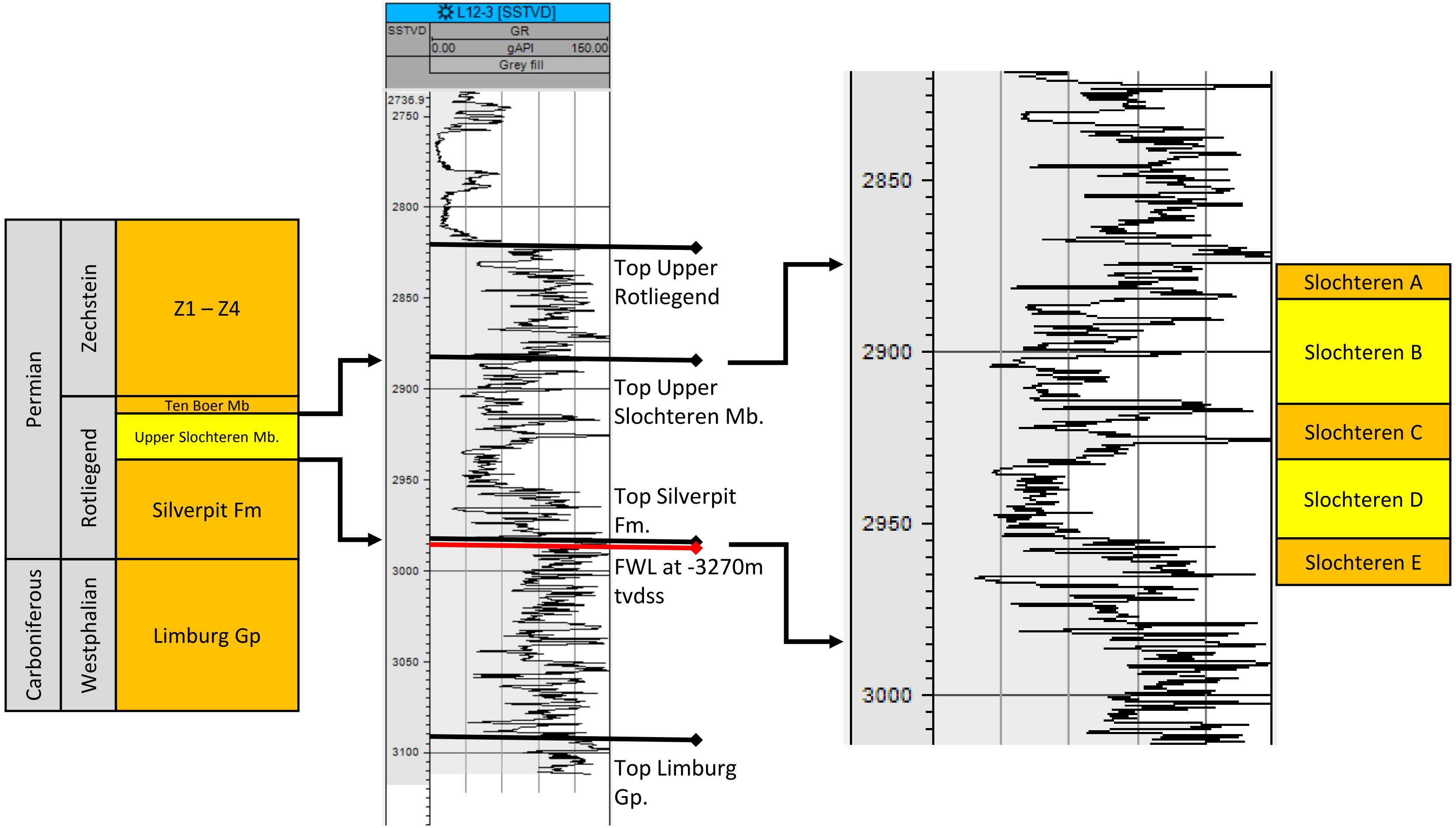

Permian
Carboniferous
Zechstein
Rotliegend
Westphalian
Z1 – Z4
Ten Boer Mb
Upper Slochteren Mb.
Silverpit Fm
Limburg Gp
L12-3 [SSTVD]
SSTVD
GR
0.00
gAPI
150.00
Grey fill
2736.9
2750
2800
2850
2900
2950
3000
3050
3100
Top Upper Rotliegend
Top Upper Slochteren Mb.
Top Silverpit Fm.
FWL at -3270m tvdss
Top Limburg Gp.
2850
2900
2950
3000
Slochteren A
Slochteren B
Slochteren C
Slochteren D
Slochteren E

Figure 11

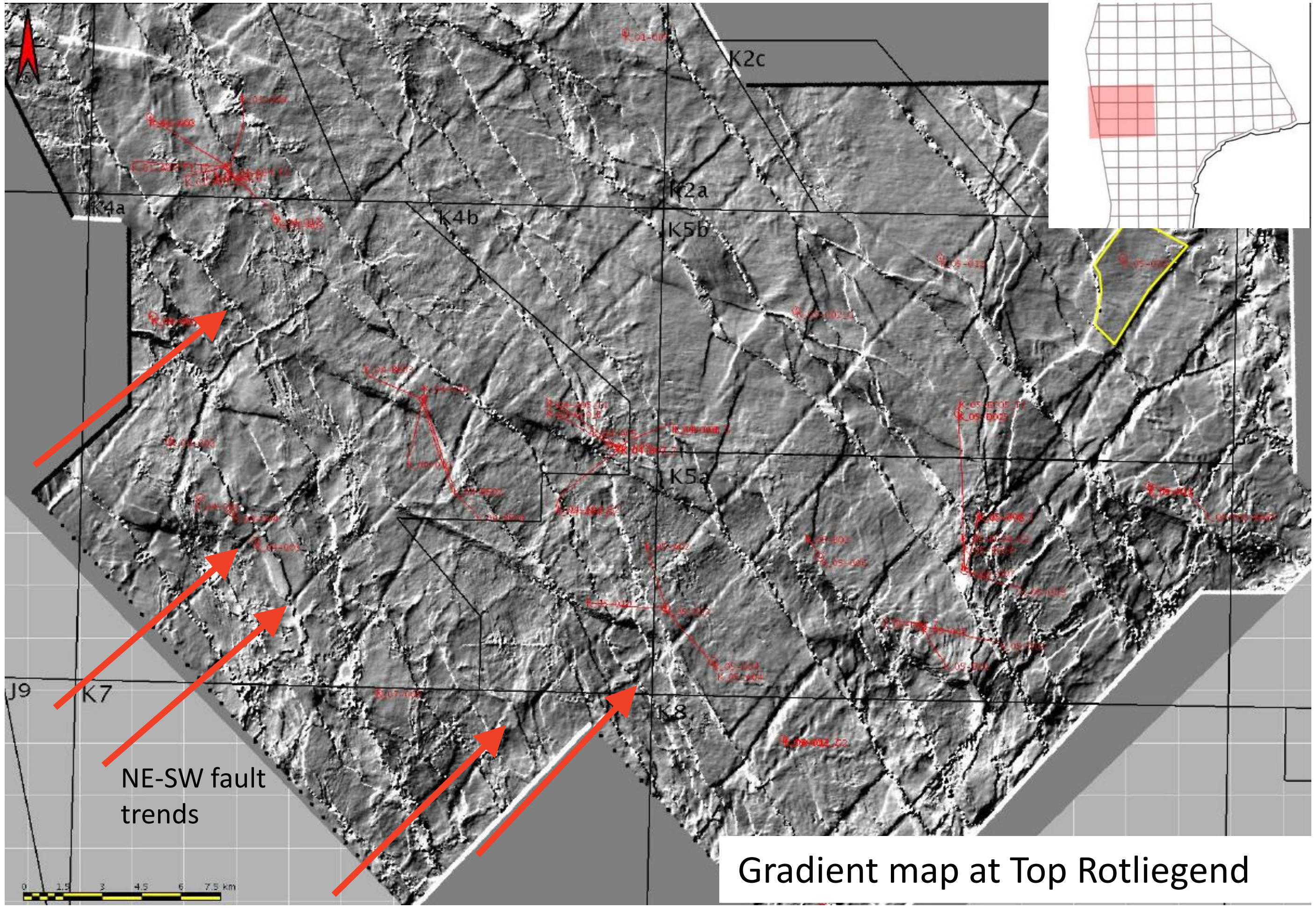
K2c
K2a
K4a
K4b
K5b
K5a
J9
K7
K8
NE-SW fault
trends
0 1.5 3 4.5 6 7.5 km
Gradient map at Top Rotliegend

Figure 5

L12b-C

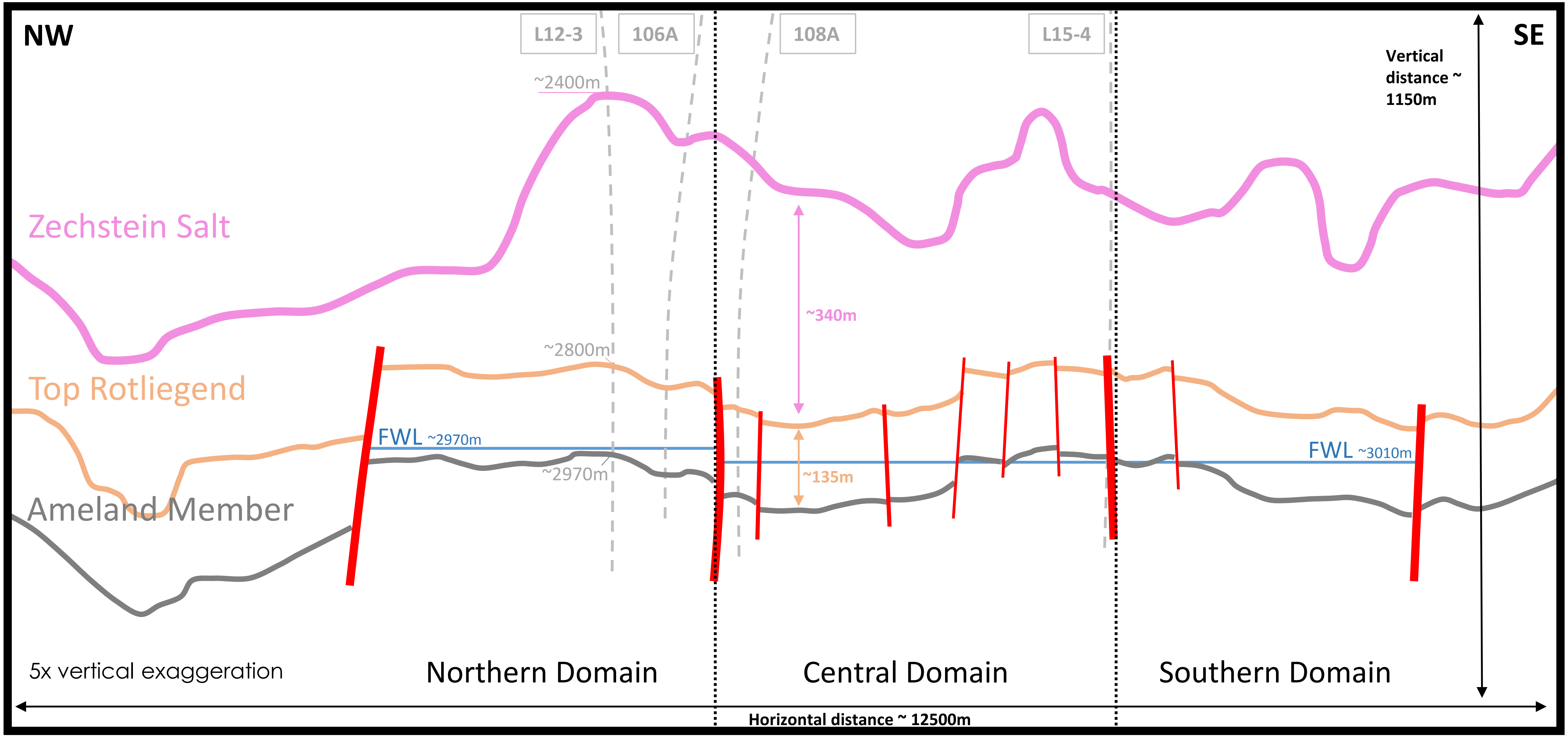

Figure 12

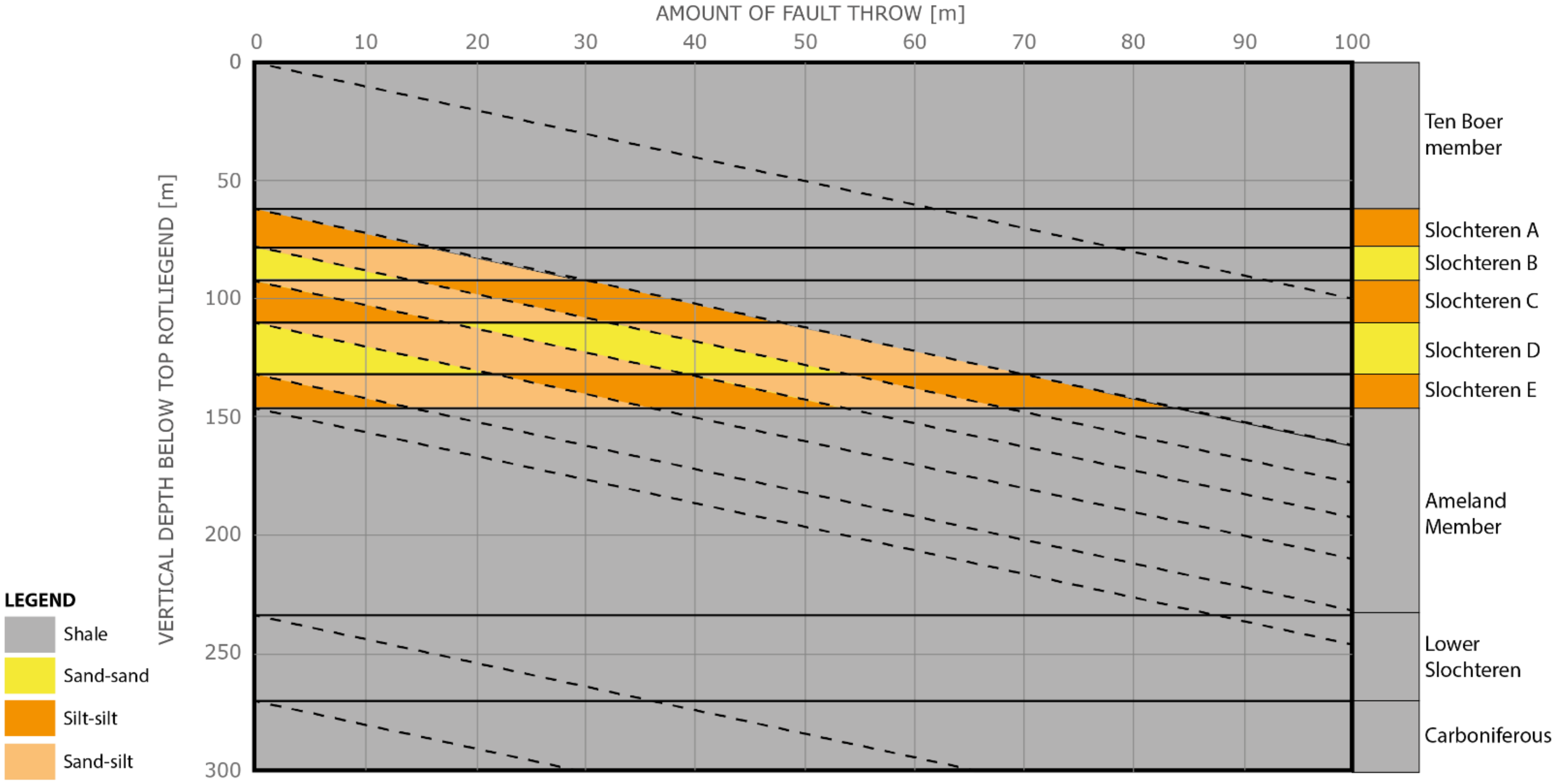
AMOUNT OF FAULT THROW [m]
0
10
20
30
40
50
60
70
80
90
100
VERTICAL DEPTH BELOW TOP ROTLIEGEND [m]
0
50
100
150
200
250
300
Ten Boer member
Slochteren A
Slochteren B
Slochteren C
Slochteren D
Slochteren E
Ameland Member
Lower Slochteren
Carboniferous
LEGEND
Shale
Sand-sand
Silt-silt
Sand-silt

Figure 13

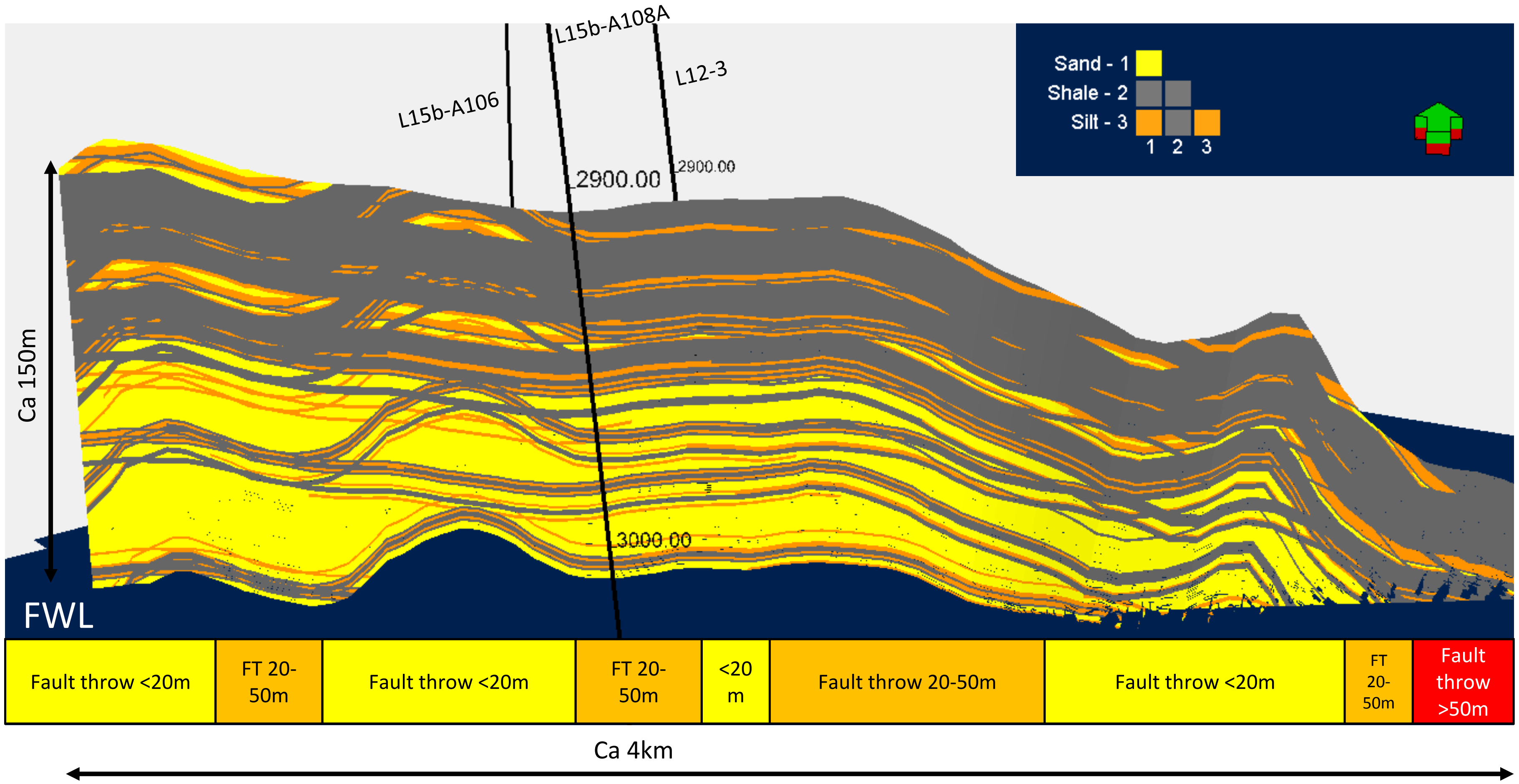
L15b-A106
L15b-A108A
L12-3
2900.00
2900.00
3000.00
Sand - 1
Shale - 2
Silt - 3
1 2 3
Ca 150m
FWL
Fault throw <20m
FT 20-50m
Fault throw <20m
FT 20-50m
<20 m
Fault throw 20-50m
Fault throw <20m
FT 20-50m
Fault throw >50m
Ca 4km

Figure 14

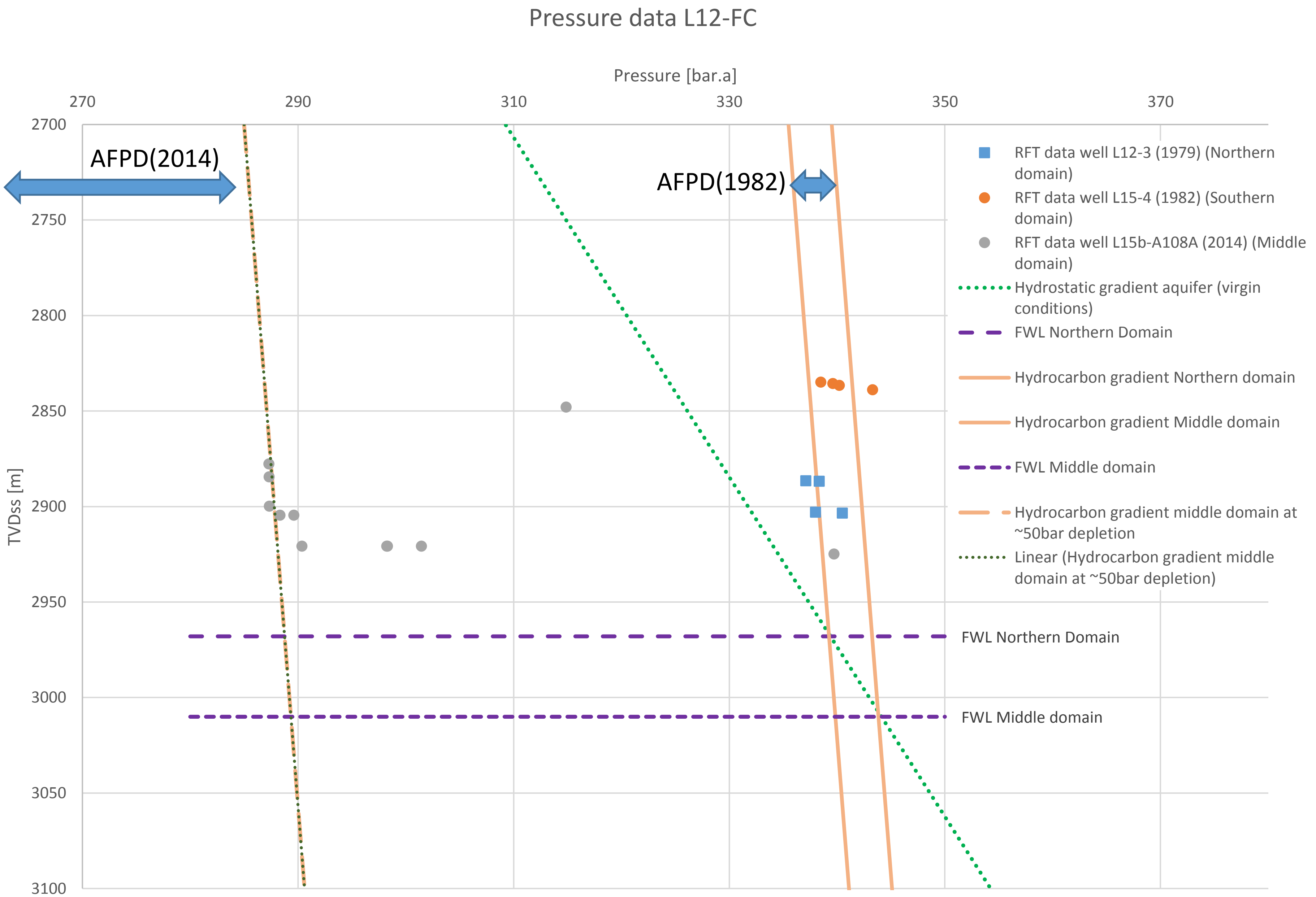

Pressure data L12-FC
Pressure [bar.a]
270
290
310
330
350
370
2700
2750
2800
2850
2900
2950
3000
3050
3100
TVDss [m]
AFPD(2014)
AFPD(1982)
RFT data well L12-3 (1979) (Northern domain)
RFT data well L15-4 (1982) (Southern domain)
RFT data well L15b-A108A (2014) (Middle domain)
Hydrostatic gradient aquifer (virgin conditions)
FWL Northern Domain
Hydrocarbon gradient Northern domain
Hydrocarbon gradient Middle domain
FWL Middle domain
Hydrocarbon gradient middle domain at ~50bar depletion
Linear (Hydrocarbon gradient middle domain at ~50bar depletion)
FWL Northern Domain
FWL Middle domain

Figure 15

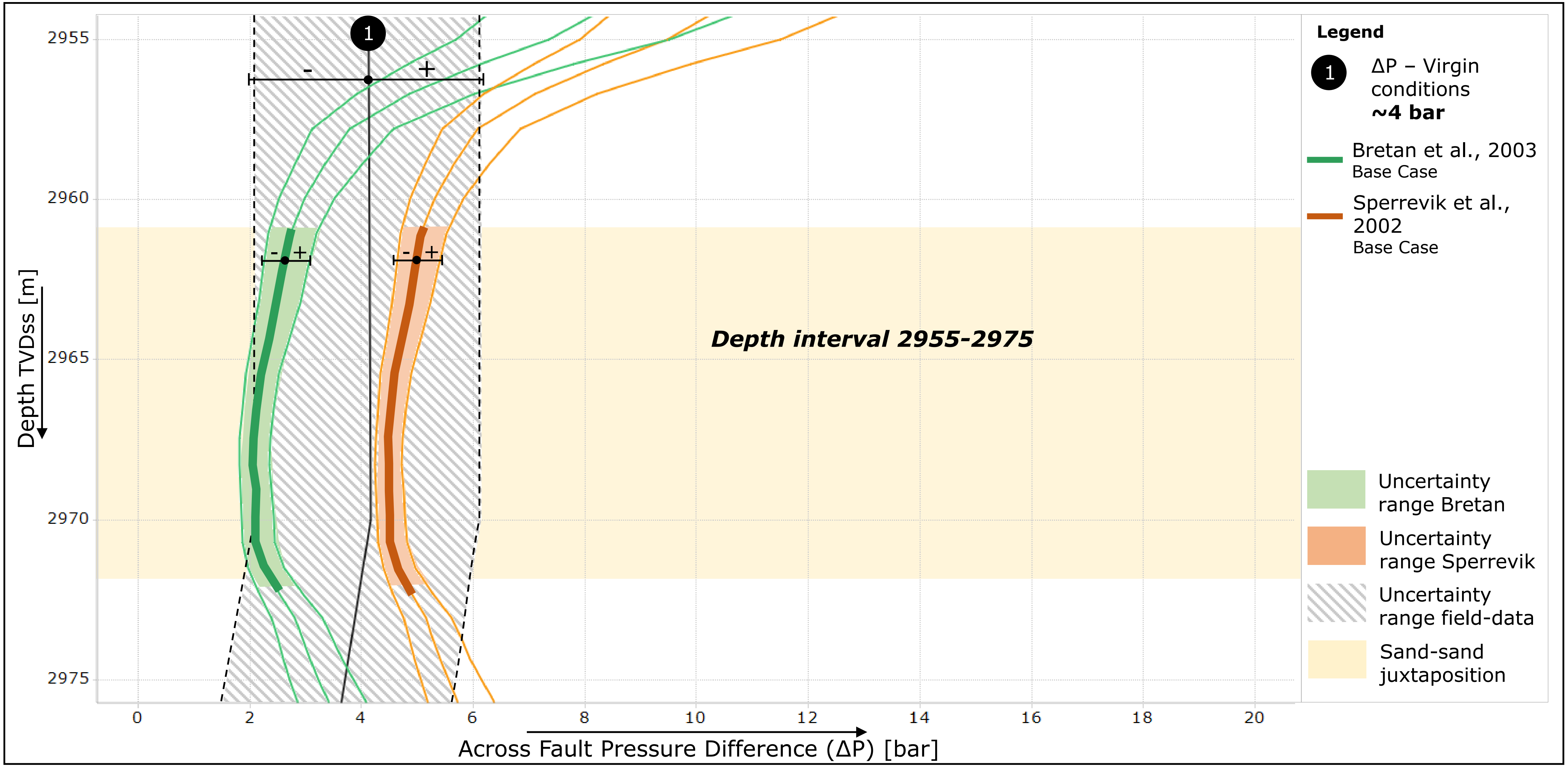

1
-
+
Depth interval 2955-2975
Depth TVDss [m]
2955
2960
2965
2970
2975
0
2
4
6
8
10
12
14
16
18
20
Across Fault Pressure Difference (ΔP) [bar]
Legend
ΔP – Virgin conditions
~4 bar
Bretan et al., 2003
Base Case
Sperrevik et al., 2002
Base Case
Uncertainty range Bretan
Uncertainty range Sperrevik
Uncertainty range field-data
Sand-sand juxtaposition

Figure 16

Figure 17

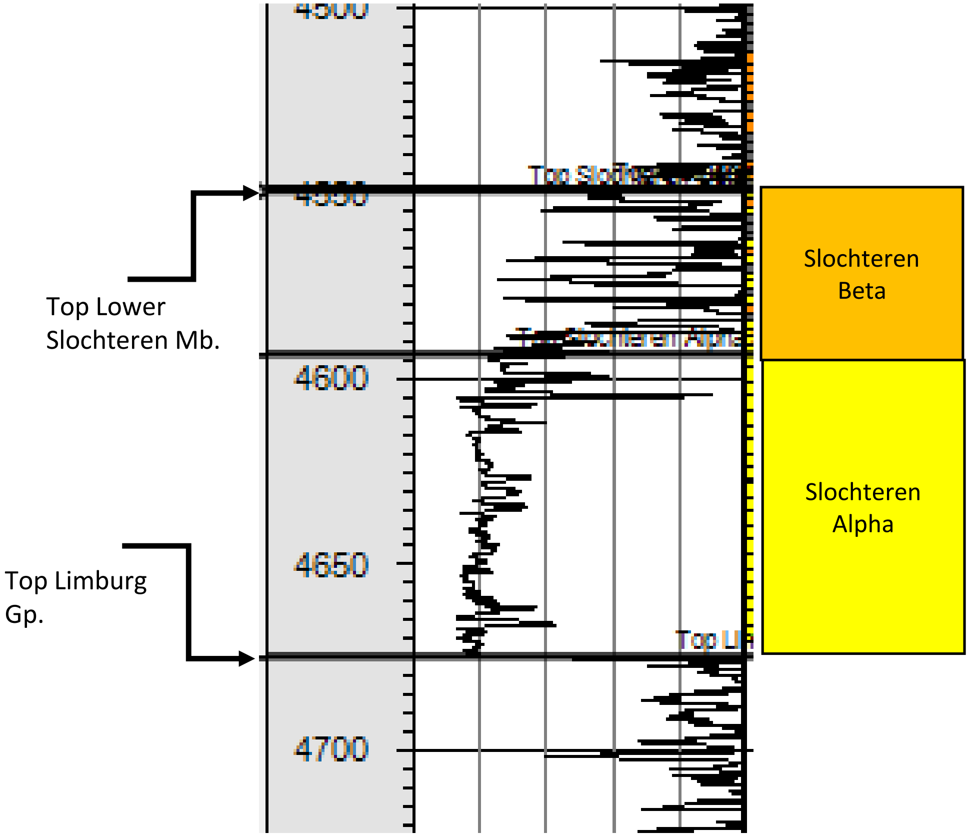
4550
4600
4650
4700
Top Lower Slochteren Mb.
Top Limburg Gp.
Slochteren Beta
Slochteren Alpha
Top Slochteren Alpha

Figure 18

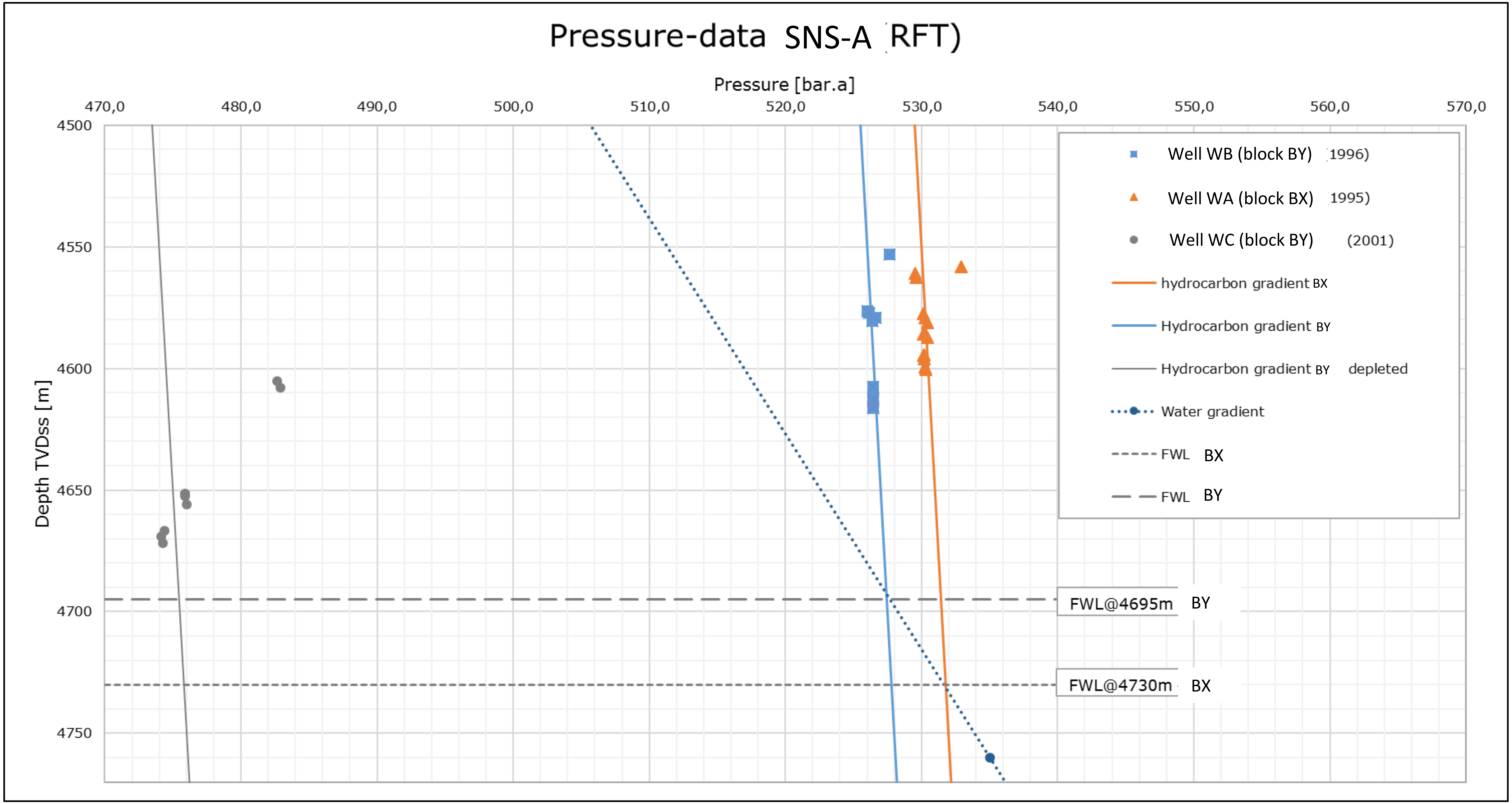

Pressure-data SNS-A RFT)
Pressure [bar.a]
470,0
480,0
490,0
500,0
510,0
520,0
530,0
540,0
550,0
560,0
570,0
4500
4550
4600
4650
4700
4750
Depth TVDss [m]
Well WB (block BY) 1996)
Well WA (block BX) 1995)
Well WC (block BY) (2001)
hydrocarbon gradient BX
Hydrocarbon gradient BY
Hydrocarbon gradient BY depleted
Water gradient
FWL BX
FWL BY
FWL@4695m BY
FWL@4730m BX

Figure 19

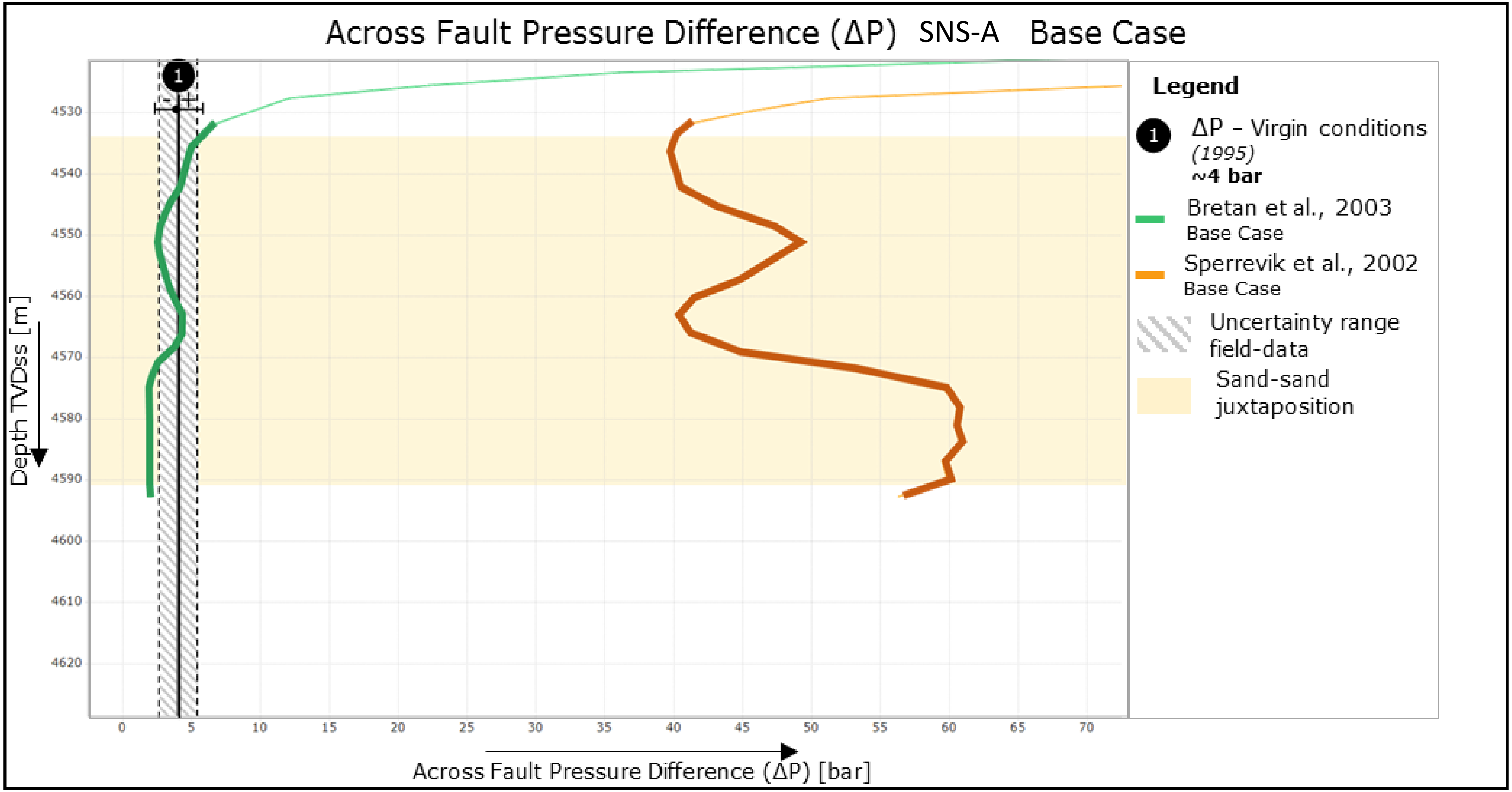
Across Fault Pressure Difference (ΔP) SNS-A Base Case
Depth TVDss [m]
4530
4540
4550
4560
4570
4580
4590
4600
4610
4620
0
5
10
15
20
25
30
35
40
45
50
55
60
65
70
Across Fault Pressure Difference (ΔP) [bar]
1
Legend
ΔP - Virgin conditions
(1995)
~4 bar
Bretan et al., 2003
Base Case
Sperrevik et al., 2002
Base Case
Uncertainty range
field-data
Sand-sand
juxtaposition

Figure 20

Click here to access/download
dataset
Draft paper fault sealing v6 - Datasets.docx